RUNX2/miR-31/SATB2 pathway in nickel-induced BEAS-2B cell transformation

YUSHA ZHU[1], QIAO YI CHEN[2], ASHLEY JORDAN[1], HONG SUN[1], NIRMAL ROY[1] and MAX COSTA[1]

[1]Department of Environmental Medicine, New York University Grossman School of Medicine, New York, NY 10100, USA; [2]Department of Cell Biology and Genetics, School of Basic Medical Sciences, Xi'an Jiaotong University Health Science Center, Xi'an, Shanxi 710000, P.R. China

Received January 26, 2021; Accepted May 5, 2021

DOI: 10.3892/or.2021.8105

Abstract. Nickel (Ni) compounds are classified as Group 1 carcinogens by the International Agency for Research on Cancer (IARC) and are known to be carcinogenic to the lungs. In our previous study, special AT-rich sequence-binding protein 2 (SATB2) was required for Ni-induced BEAS-2B cell transformation. In the present study, a pathway that regulates the expression of SATB2 protein was investigated in Ni-transformed BEAS-2B cells using western blotting and RT-qPCR for expression, and soft agar, migration and invasion assays for cell transformation. Runt-related transcription factor 2 (RUNX2), a master regulator of osteogenesis and an oncogene, was identified as an upstream regulator for SATB2. Ni induced RUNX2 expression and initiated BEAS-2B transformation and metastatic potential. Previously, miRNA-31 was identified as a negative regulator of SATB2 during arsenic-induced cell transformation, and in the present study it was identified as a downstream target of RUNX2 during carcinogenesis. miR-31 expression was reduced in Ni-transformed BEAS-2B cells, which was required to maintain cancer hallmarks. The expression level of miR-31 was suppressed by RUNX2 in BEAS-2B cells, and this increased the expression level of SATB2, initiating cell transformation. Ni caused the repression of miR-31 by placing repressive marks at its promoter, which in turn increased the expression level of SATB2, leading to cell transformation.

Introduction

Nickel (Ni) compounds are classified as Group 1 carcinogens by the International Agency for Research on Cancer. Previous studies reported that workers processing and refining sulfidic nickel ores have increased risk of pulmonary and sinonasal cancers (1-6). Previously, special AT-rich sequence-binding protein (SATB2), a nuclear matrix-associated protein, was identified as the only common gene upregulated in BEAS-2B cells transformed by nickel, arsenic, vanadate, and hexavalent chromium (7). It is a member of the family of special AT-rich sequence-binding proteins and is an embryonic gene important in regulating stem cell differentiation and development (8). SATB2 overexpression has been observed in numerous cancers, such as colon, breast, ovarian, lung, and sinonasal carcinomas (9-12). SATB2 has been increasingly studied in cancer development and is considered to be a biomarker for colon cancer (9,13). SATB2 is upstream of numerous prognostic markers of colorectal cancer (CRC) such as acyl-CoA synthetase long-chain 6 (ACSL6) and Vav guanine nucleotide exchange factor 3 (VAV3) (14). Numerous downstream targets of SATB2 such as Bcl-2, Bsp, c-Myc, Klf4, Hoxa2 and Nanog are also important regulators of cell pluripotency and survival (15). Thus, it is considered that inappropriate induction of SATB2 in normal mammalian cells may act as a driver of cell transformation.

In fact, the critical role of SATB2 in Ni-induced BEAS-2B cell transformation has been identified (16) and in the present study the upstream regulators for SATB2 signaling were investigated. Runt-related transcription factor 2 (RUNX2) is a master regulator of osteogenesis and it has a number of overlapping functions with SATB2 (17,18). The interaction between RUNX2 and SATB2 in osteogenesis has been identified in several previous studies (19-26). RUNX2 was detected in a limited number of non-osseous tissues, while increased expression of RUNX2 has been described in the progression and metastasis of several human cancers. Overexpression of RUNX2 was observed in prostate, pancreatic, breast, thyroid, and bone cancers (27-30). Increased expression of RUNX2 suppressed microRNA (miRNA or miR)-31 allowing SATB2 protein translation and initiation of carcinogenesis. Moreover, genes located downstream of RUNX2, such as matrix metalloproteinases (MMPs), vascular epithelial growth factor (VEGF), bone sialoprotein (BSP) and c-Myc were also involved in promoting cancer cell metastasis (31-34). Genes such as SRY-box transcription factor 9 (SOX9), snail family transcriptional repressor 2 (SNAI2), snail family transcription repression 3 (SNAI3), twist family bHLH transcription

Correspondence to: Dr Max Costa, Department of Environmental Medicine, New York University Grossman School of Medicine, 341 East 25th Street, New York, NY 10100, USA
E-mail: max.costa@nyulangone.org

Key words: carcinogenesis, runt-related transcription factor 2, special AT-rich sequence-binding protein 2, miRNA, nickel

factor 1 (TWIST1) and SMAD family member 3 (SMAD3) regulated by RUNX2 induced cell invasion (35,36). RUNX2 modulated SATB2 expression by suppressing the expression of miRNAs that directly target SATB2 mRNA in both osteogenesis and carcinogenesis (22,23,26,37-41). Expression of RUNX2 appears to be a critical upstream event leading to the increase of SATB2 and transforming BEAS-2B cells.

miRNAs are small noncoding RNAs that are known to mediate mRNA degradation and inhibit translation of proteins as well as altering chromatin structure during early development, differentiation, metabolic control and cell death (42-45). The expression of miRNAs has been revealed to be globally suppressed in tumors (46). Several studies have reported that altered miRNA expression is involved in various stages of Ni carcinogenesis (47). SATB2 has been revealed to be negatively regulated by several miRNAs that target its 3'-untranslated region (UTR) during osteogenesis and carcinogenesis, including miR-211, miR-31, miR-23a/27a/24-2 cluster, miR-499, miR-34c, miR-875, miR-599 (10,23,37,38,40,48-54). miR-31 was identified as a negative regulator for SATB2 in arsenic-induced BEAS-2B transformation (40). In fact, miR-31 was also targeted by RUNX2 and miR-31 allowed RUNX2 to regulate and increase SATB2 during osteogeneses (21,22). The aim of the study was to investigate whether RUNX2 is an upstream regulator for SATB2, mediating Ni-induced BEAS-2B cell transformation by regulating the expression level of miR-31. This carcinogenic pathway mirrors what occurs during normal bone development.

Materials and methods

Cells and cell culture. BEAS-2B human bronchial epithelial cells were obtained from the American Type Culture Collect (ATCC). Before the start of the present study, the cells were examined at Genetica DNA Laboratories and were revealed to be 100% authentic against a reference BEAS-2B cell line (ATCC CRL-9609). Cells were cultured in Dulbecco's modified Eagle's medium (DMEM, Invitrogen; Thermo Fisher Scientific, Inc.) supplemented with 10% fetal bovine serum (FBS; Atlanta Biologicals, Inc.; R&D Systems, Inc.) and 1% penicillin/streptomycin (Gibco; Thermo Fisher Scientific, Inc.) at 37˚C in an atmosphere containing 5% CO_2.

Ni-transformed (Ni-T) BEAS-2B cells were developed by chronic exposure to 0.25 mM $NiSO_4$ for 4 weeks (7). Cells were seeded by single cell suspension into soft agar and colonies were isolated and grown in monolayer on culture dishes. Each clone was analyzed using Affymetrix gene expression arrays and the clones with highest SATB2 expression were selected for the present study. The Ni-T cells were maintained in DMEM supplemented with 10% FBS and 1% p/s at 37˚C in a humidified incubator containing 5% CO_2.

Stable overexpression and knockdown. Stable overexpression of miR-31 in Ni-T cells was achieved using miR-31 construct (cat. no. HmiR0138-MR04-10), which was purchased from GeneCopoeia, Inc. RUNX2 plasmid constructs (clone ID OHU22872D) were acquired from Genscript. Short hairpin (sh)-RUNX2 (cat. no. HSH021333-CU6; scrambled control ID CSHCTR001-1-CU6.1) and miR-31 inhibitor plasmid (cat. no. HmiR-AN0401-AM01; control ID CmiR-AN0001-AM01) were obtained from GeneCopoeia, Inc. The sequence for sh-RUNX2 and sh-miR-31 were as follows: sh-RUNX2-a: 5'-GCAGCACGCTATTAAATCCAA-3'; sh-RUNX2-b: 5'-GCAGAATGGATGAATCTGTTT-3'; sh-RUNX2-c: GCG ACCATATTGAAATTCCTC-3'; scrambled control: 5'-GCT TCGCGCCGTAGTCTTA-3'; sh-miR-31: 5'-AGGCAAGAU GCUGGCAUAGCU-3'. Each plasmid was purified by a Qiagen QIAprep Spin Miniprep kit (cat. no. 27104) before transfection, using the Lipofectamine™ LTX reagent with PLUS kit (cat. no. 15338030; Invitrogen; Thermo Fisher Scientific, Inc.) used according to the manufacturer's instructions. Briefly, the cells were plated in 2 ml growth medium in a 6-well plate and were ~70-80% confluent during transfection. For each transfection, 2.5 μg of purified plasmid was diluted in 250 μl Opti-MEM. Immediately before transfection, 2.5 μl PLUS reagent was added to the diluted plasmid. Then, 10 μl Lipofectamine™ LTX reagent was diluted in 250 μl Opti-MEM and then mixed with the plasmid and PLUS reagent. The mixture was incubated for 5 min at room temperature before adding into the well. The medium was replaced with fresh complete DMEM 24 h after transfection. The cells were divided onto 10 cm^2 dishes 48 h after transfection and selection reagents (500 μg/ml hygromycin or 0.5 μg/ml puromycin) were added. After selection for 2 weeks (hygromycin) or 3 days (puromycin), the pooled clones were harvested for western blotting and RT-qPCR analysis.

RNA extraction and reverse transcription-quantitative (RT-q) PCR. Cells were lysed by TRI-reagent (Molecular Research Center, Inc.) (1 ml/well of a 6-well plate). RNA was extracted using 200 μl chloroform (Sigma-Aldrich; Merck KGaA) and centrifuged at 13,000 x g for 10 min at 4˚C, separating the RNA in the aqueous phase. RNA was then precipitated by 500 μl isopropanol and washed twice with 750 μl of 75% ethanol. RNA pellets were obtained by centrifugation for 5 min at 13,000 x g at 4˚C and air-dried for 10 min. RNA was solubilized in RNase-free water and heat-inactivated at 65˚C for 10 min.

Single-strand cDNA was generated from 250 ng RNA by First Strand cDNA Synthesis kit (cat. no. E6300; New England Biolabs, Inc.) using random primers according to the manufacturer's instructions. The primer and RNA mix were denatured at 70˚C for 5 min. Reaction enzyme and buffer were mixed at a ratio of 1:5 and added into each sample for cDNA synthesis. Samples were incubated at 25˚C for 5 min, followed by cDNA synthesis reaction at 42˚C for 1 h and then the enzymes were inactivated at 80˚C for 5 min. Quantitative PCR analysis was performed by SYBR green qPCR Master Mix (Roche Diagnostics). A total of 4 ng cDNA product and master mix were added into each well of a 384-well plate. The reaction was performed on an ABI PRISM 7900HT system (Applied Biosystems; Thermo Fisher Scientific, Inc.) and each sample was run in triplicate. The thermocycling conditions were as follows: 95˚C for 10 min, 30 cycles at 95˚C for 15 sec and 60˚C for 1 min, and 72˚C for 10 min. Relative gene expression level was quantified using the $2^{-\Delta\Delta Cq}$ method (55) and normalized to the expression of the house-keeping gene glyceraldehyde 3-phosphate dehydrogenase (GAPDH).

miRNA extraction was performed according to the manufacturer's instructions using the miRVana RNA isolation kit

(cat. no. AM1560, Invitrogen; Thermo Fisher Scientific, Inc.) and quantified by a NanoDrop spectrophotometer. cDNA was synthesized using a TaqMan microRNA reverse transcription kit (cat. no. 4366596; Thermo Fisher Scientific, Inc.) for miR-31, according to the manufacturer's instructions. The relative expression level was normalized to the expression of U6. Finally, qPCR analysis was conducted by TaqMan primers (Thermo Fisher Scientific, Inc.) on an 7900HT system (Applied Biosystems; Thermo Fisher Scientific, Inc.). The thermocycling conditions were as follows: 95˚C for 10 min, 40 cycles at 95˚C for 15 sec and 60˚C for 1 min. Primers were designed using the Primer Expression Software (v3.0.1; Thermo Fisher Scientific, Inc.) and the sequences were as follows: RUNX2 forward, 5'-GAGTCCTTCTGTGGCATGCA-3' and reverse, 5'-TGGCCTGGTGGTGTCATTAG-3'; SATB2 forward, 5'-TCTCCCCAAACACACCATCA-3' and reverse, 5'-GCAGCTCCTCGTCCTTATATTCA-3'; SIRT6 forward, 5'-TTTTTCTCTCGTGGTCTCACTTTGT-3' and reverse, 5'-ACGGAGGGCAGGTGTAACC-3'; BSP forward, 5'-AAAGTGAGAACGGGGAACCTT-3' and reverse, 5'-GATGCAAAGCCAGAATGGAT-3'; VEGF forward, 5'-CTTGCCTTGCTGCTCTAC-3' and reverse, 5'-TGGCTTGAAGATGTACTCG-3'; GAPDH forward, 5'-TGCACCACCAACTGCTTAGC-3' and reverse, 5'-GGCATGGACTGTGGTCATGA-3'; miR-31 promoter A forward, 5'-TGCTATCTGCAGTACTGTGCTGAGG-3' and reverse, 5'-AGAGAGGCTGTGGTTAGTTCCTGCT-3'; miR-31 promoter B forward, 5'-ACTGCCTTGACTTCCTGCCTTGGTG-3' and reverse, 5'-TAGCTAGGTCTGTACCCTGTCTCAG-3'.

Western blot analysis. Cells were washed with PBS and lysed by heating in boiling buffer (1% SDS, 10 mM Tris-HCl pH 7.4, 1 mM sodium orthovanadate). Samples were boiled at 100˚C for 10 min and sonicated on high for 15 min at 4˚C. The cell debris was removed by 13,000 x g centrifugation for 20 min at 4˚C and the supernatant was collected. The protein concentration was analyzed using the Bradford Protein Assay (Bio-Rad Laboratories, Inc.). A total of 5 different dilutions of bovine serum albumin (BSA) (Sigma-Aldrich; Merck KGaA) were prepared in boiling buffer to create the standard curve. The absorbance was measured at 595 nm on spectrophotometer SpectraMax M2 (Molecular Devices, LLC). Samples (30 μg each) were mixed with a 6X SDS sample buffer (375 mM Tris-HCl pH 6.8, 6% SDS, 4.8% glycerol, 9% 2-mercaptoethanol, 0.03% bromophenol blue) and separated on a 10% SDS-PAGE. The proteins were then transferred onto a 0.45-μm nitrocellulose membrane at 100 V for 60 min. After blocking with 5% skimmed milk in TBS for 30 min at room temperature, the membrane was incubated with primary antibody in 5% milk/TBS solution overnight at 4˚C. The primary antibodies used were: Anti-RUNX2 (1:200; product no. sc101145; Santa Cruz Biotechnology, Inc.) anti-SATB2 (1:100; product no. ab51502; Abcam) and anti-β-actin (1:1,000; product no. 3700S; Cell Signaling Technology, Inc.).

The membrane was washed with TBST (Tris-buffered saline with 0.1% Tween-20 detergent) for 5 min 3 times before horseradish peroxidase (HRP)-labeled secondary antibody incubation for 1 h at room temperature. The secondary antibodies used were as follows: HRP-conjugated anti-mouse (1:2,000 dilution; cat. no. sc-516102; Santa Cruz Biotechnology, Inc.); or HPR-conjugated anti-rabbit (1:2,000 dilution; cat. no. sc-2357; Santa Cruz Biotechnology, Inc.). The protein bands were visualized by the chemiluminescence after incubating the membrane in an enhanced-chemiluminescence (ECL) reagent (Thermo Fisher Scientific, Inc.) for 2 min at room temperature and imaging films were developed by an OPTIMAX X-Ray Film Processor (Merry X-Ray Corporation). To control for sample loading and protein transfer, β-actin was probed as an internal reference control. Quantification of immunodetected protein bands was performed by ImageJ software (V1.53e, National Institutes of Health).

Soft agar assay. Approximately 5,000 cells were mixed in a top layer of 0.35% 2-hydroxyethylagarose (Type VII low gelling temperature; Sigma-Aldrich; Merck KGaA)/DMEM upon a bottom layer of 0.5% 2-hydroxethylagarose/DMEM in a 6-well plate. A total of 200 cells for each sample were seeded onto a 10 cm^2 dish and cultured for two weeks to assess plating efficiency. The colonies in the plates were stained by 5% Giemsa solution (40% methanol/60% glycerol) for ~4 h at room temperature (Thermo Fisher Scientific, Inc.) and the number of colonies were determined. The cells in agarose were humidified with 200 μl DMEM for each well twice a week and cultured for four weeks until individual colonies were visible under the light microscope at a magnification of x20. Each well was stained with 0.1% INT/BCIP solution (Roche Diagnostics) in 0.1 M Tris/0.05 M $MgCl_2$/0.1 M NaCl at 4˚C overnight, and images were captured by a Bio-Rad Molecular Imager Gel-Doc XR+ system and analyzed on the Image Lab software (v2.0.1 build 18; Bio-Rad Laboratories, Inc.). The number of colonies were counted by ImageJ software using defined particle size of 6-infinity pixel units and circularity of 0.30-1.00.

Scratch test. Cells were plated onto gridded plates (2x2 mm grids on the bottom) (Nalge Nunc International). Upon reaching 90-100% confluency, cells were washed with PBS twice and a single scratch was produced across the monolayer between the grids by a 200-μl pipette tip held perpendicular to the plate bottom. The plates were gently washed with PBS to remove detached cells and cells were then maintained in serum-free medium to inhibit proliferation that might interfere with measurement of cell migration. For the CADD522 group, cells were cultured in medium containing 50 μM CADD522 during this experiment. CADD522 is a small molecule inhibitor for RUNX2, and it was kindly provided by Dr. Antonino Passaniti from University of Maryland School of Medicine (Baltimore, MD, USA). Images were captured every 24 h after the scratch using a Nikon digital DS-Fil1-U3 camera linked with a microscope by bright field light at a magnification of x20 and controlled by NIS-Elements F3.2 software on a Nikon Eclipse TS100 microscope (Nikon Corporation). The wound healing rate was estimated by calculating the percentage of the area of the wound covered or migrated during 48 h in the image (wound area at 0 h-wound area at 48 h)/wound area at 0 h x100%) measured by ImageJ software (v1.53e).

Invasion assay. The Matrigel-coated invasion chambers (Corning, Inc.) were placed in a 24-well plate and balanced with low serum medium (0.1% FBS/DMEM) at 37˚C for 3 h.

The medium was carefully removed, and the lower wells were filled with 1 ml 10% FBS/DMEM. Cells were washed with PBS twice and $5x10^4$ cells were suspended in 400 μl of 0.1% FBS/DMEM and seeded into each upper chamber. For the CADD522 group, cells were pretreated with 50 μM CADD522 for 24 h at 37˚C and the medium in the chamber contained 50 μM CADD522. After culturing for 24 h, Transwell chambers were washed with PBS and fixed by 10% formalin for 5 min and methanol for 20 min at room temperature. The membranes in the bottom chambers were stained with 10% Giemsa overnight at room temperature and washed with H_2O three times on the following day. Non-invasive cells were inside of the chamber and were gently removed by wet cotton swabs. The images were captured with a bright field light microscope at a magnification of x20 controlled by NIS-Elements F3.2 software on a Nikon Eclipse TS100 microscope. Three fields were randomly selected for each chamber membrane and the number of invading cells were determined by ImageJ software (v1.53e).

Cell viability and cytotoxicity assay. Cell viability and cytotoxicity were assessed by the CellTiter-Fluor Cell Viability Assay kit and CytoTox-Fluor Cytotoxicity Assay kit (cat. nos. G6080 and G9260, respectively; both from Promega Corporation) used according to the manufacturer's instructions. Cells were seeded onto a 96-well plate and then treated with CADD522 at the indicated time-point and doses (25, 50, 100, 150 and 300 μg/ml for 48 h, respectively). Each treatment was repeated 4 times. GF-AFC substrate and bis-AAF-R110 substrate were diluted (200X) in the indicated assay buffers and mixed with culture media at a ratio of 1:5. A total of 60 μl mixture was added into each well. Plates were then incubated in the dark for 1 h at room temperature. Cell viability was measured at $400_{Ex}/505_{Em}$ nm, and cell toxicity was assessed at $485_{Ex}/520_{Em}$ nm on a fluorescence plate.

RNA stability assay. Actinomycin D can form a stable complex with DNA and block DNA-dependent RNA polymerase activity to inhibit new mRNA synthesis, allowing measurements of mRNA decay (56). Briefly, approximately $1x10^5$ cells were seeded on a 6-well plate. For the CADD522 treatment group, cells were treated with CADD522 at 50 μg/ml for 24 h at 37˚C before collection. Cells were then treated with 10 μg/ml of actinomycin D (Invitrogen; Thermo Fisher Scientific, Inc.) for indicated time intervals (0, 8, 16 and 24 h) at 37˚C. Cells were then washed twice with PBS and collected by TRI-reagent and subjected to RNA extraction, cDNA synthesis with random primers and RT-qPCR analysis for SATB2 mRNA expression.

ChIP assay. Chromatin immunoprecipitation (ChIP) was used to confirm the binding of RUNX2 in the promoter region of miR-31. Ni-T cells were treated with 50 μM CADD522 for 48 h and were crosslinked with 1% formaldehyde (Sigma-Aldrich; Merck KGaA) in DMEM for 10 min at room temperature. The crosslink reaction was stopped by treating cells with 250 mM glycine for 5 min and were washed twice with cold PBS supplemented with 1 mM PMSF and protease inhibitors (1 tablet in 10 ml buffer; cOmplete mini EDTA-free protease inhibitor cocktail; MilliporeSigma). The ChIP Assay kit (cat. no. 17-295; MilliporeSigma) was used for immunoprecipitation of DNA-protein complexes and reverse crosslinked DNA. Briefly, cells were collected and suspended in SDS lysis buffer provided in the kit and followed by sonication at 60 kHz to shear DNA between 200 and 1,000 base pairs. The chromatin size was verified on a 2% agarose gel. Once the sonication conditions were optimized (36 cycles at 40% power), samples were then diluted in ChIP dilution buffer. The chromatin complex was then immunoprecipitated with anti-RUNX2 antibody (1:50; cat. no. ab236639; Abcam) or anti-IgG (1:50; cat. no. 12-370; Sigma-Aldrich; Merck KGaA) as a control overnight at 4˚C. The following day, Protein A Agarose/Salmon Sperm DNA (50% Slurry) was added at 4˚C and incubated for 1 h. The beads were then collected by centrifugation at 200 x g at 4˚C for 1 min to remove unbound non-specific DNA. The beads were washed in the following order: Low salt, high salt, LiCl, and TE buffer. The RUNX2 protein was then eluted from the antibody by elution buffer (1% SDS, 0.1M NaHCO3) and the protein-DNA crosslinks were reversed by heating at 65˚C for 4 h. Samples were then treated with 10 μl of 0.5 M ethylenediaminetetraacetic acid (EDTA), 20 μl of 1 M Tris-HCl, 2 μl of 10 mg/ml Proteinase K, and 5 μl of 10 mg/ml RNase A and incubated at 45˚C for 1 h to digest proteins and RNAs. DNA was then recovered by phenol/chloroform extraction and ethanol precipitation. To increase recovery of DNA, glycogen and sodium acetate were added. DNA was eluted in TE buffer and the concentration of DNA in the samples was analyzed by PicoGreen (cat. no. P7589, Invitrogen; Thermo Fisher Scientific, Inc.). For qPCR analysis, approximately 0.2 ng of DNA was used per well on 384-well plates. The Ct values were determined using the percent input method [100*2^ (Adjusted input-Ct (IP)] to calculate enrichment.

Bioinformatics. To identify the target genes for miRNA or regulator miRNAs for a particular gene, the potential interaction of the 3' UTR of the genes with miRNAs was searched and confirmed by miRNA target prediction databases TargetScanHuman v7.2 (www.targetscan.org). The promoter of miR-31 was identified by searching the FANTOM5 data website (http://fantom.gsc.riken.jp), which is based on prediction of the promoters of protein-coding genes, and the specific promoter sequence upstream from the transcription start site (TSS) of miR-31 host gene MIR31HG (RefSeq NR_027054) was obtained at Ensembl website (http://www.ensembl.org/index.html).

Statistical analysis. Experiments were performed at least three times unless otherwise indicated and statistical significance of the study was assessed using the mean ± standard deviation (SD) by the two-tailed, unpaired t-test to compare the means of two groups or a one-way ANOVA and post-hoc Tukey's test for comparison of the means of more than two groups using GraphPad Prism 8.0 software (GraphPad Software, Inc.). $P<0.05$ was considered to indicate a statistically significant difference.

Results

Ni-T BEAS-2B cells exhibit enhanced anchorage-independent growth, migration and invasion, as well as increased SATB2 and RUNX2. Ni-induced cell transformation has

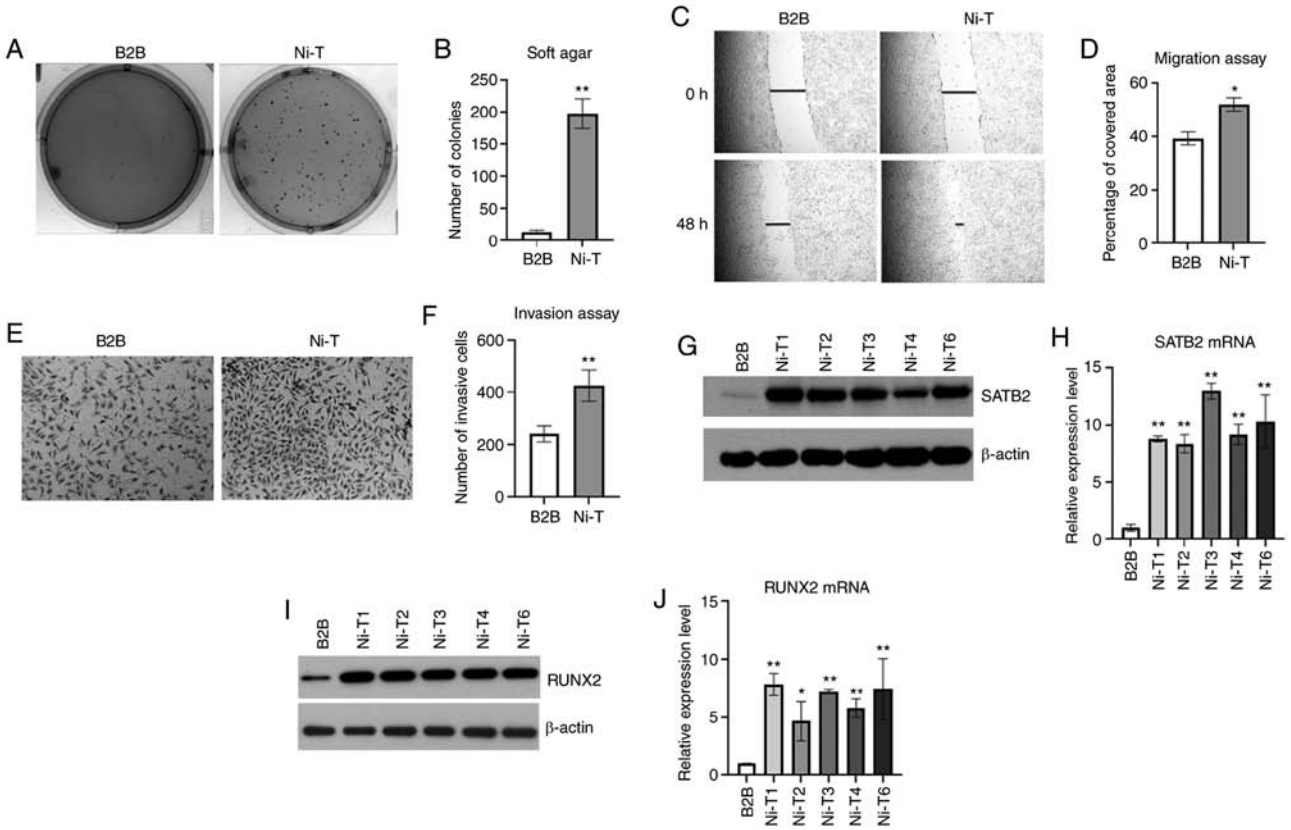

Figure 1. Ni-transformed cells exhibit increased anchorage independent growth, migration, and invasion, as well as increased SATB2 and RUNX2 levels. (A and B) Soft agar assays of Ni-T cells compared with normal BEAS-2B cells, and quantified number of colonies in agar of each group by ImageJ. (C and D) Cell migration of Ni-T cells was assessed by scratch wound healing assays and the images were captured at a magnification of x20. Quantification of wound healing rate was conducted by measuring the percentage of wound area covered for each group during 48 h using ImageJ software. (E and F) The invasion of Ni-T cells was measured by Transwell assay and the images were captured at a magnification of x20. The number of invasive cells was counted using ImageJ software and was compared with the control. (G and H) The expression levels of SATB2 protein and mRNA in normal BEAS-2B cells and in Ni-T clones were determined by western blotting and RT-qPCR assays. (I and J) The expression levels of RUNX2 protein and mRNA in normal BEAS-2B cells and in Ni-T clones were determined by western blotting and RT-qPCR assays. Statistical significance was calculated by the GraphPad Prism software using ANOVA for comparisons among groups. *P<0.05 and **P<0.01. SATB2, AT-rich sequence-binding protein 2; RUNX2, runt-related transcription factor 2; Ni-T, Ni-transformed; RT-qPCR, reverse transcription-quantitative PCR; B2B, BEAS-2B.

been documented in numerous cell studies (7,57-63). Ni-T human lung epithelial cells were obtained following four weeks of chronic exposure to 0.25 mM $NiSO_4$ and isolated from colonies that grew in soft agar (7). As demonstrated in Fig. 1A and B, Ni-T cells exhibited increased colony growth in agar compared with normal BEAS-2B cells, indicating the acquisition of anchorage-independent growth. Cellular anchorage-independent growth in the soft agar matrix implies malignant transformation (64). Cell migration and invasion are key processes for cancer metastasis and are also hallmarks of malignancy (65). Cell migration ability was determined by the scratch test. Cell invasion was assessed by culturing cells in invasion chambers coated with Matrigel matrix, which only allows cells with metastatic ability to invade and transfer (66). As revealed in Fig. 1C-F, Ni-T cells demonstrated higher wound-healing capacity and increased cell invasion compared with normal BEAS-2B cells.

In previous studies, SATB2 was indicated to be an important mediator of Ni-induced cell transformation (7,16). It was reported that knockdown of SATB2 in Ni-T cells reduced anchorage-independent growth, cell migration, and tumor formation in nude mice (16). SATB2 mRNA and protein levels were significantly increased in Ni-T cells (Fig. 1G and H). To further study the mechanisms of SATB2 induction, RUNX2 levels were measured, as the latter is an upstream regulator for SATB2. RUNX2 was revealed as a master regulator for osteogenesis in mesenchymal stem cells (67). It is not commonly expressed in normal mammalian cells, but it has been revealed to be increased in numerous cancers (68). RUNX2 indirectly regulates SATB2 expression by inhibiting miRNAs in both osteogenesis and cancers. The mRNA and protein levels of RUNX2 were examined in Ni-T cells. As revealed in Fig. 1I and J, the expression of RUNX2 was increased as compared with control BEAS-2B cells, indicating a possible role of RUNX2 in Ni-mediated induction of SATB2.

Overexpression of RUNX2 promotes cancer hallmarks in BEAS-2B cells. RUNX2 appears to be an upstream regulator of SATB2. To investigate whether SATB2 can be induced by RUNX2 in BEAS-2B cells, RUNX2 was stably overexpressed in BEAS-2B cells (Fig. 2A and B). The mRNA and protein levels of SATB2 were increased by expressing RUNX2 (Fig. 2A and C). Overexpression of SATB2 in BEAS-2B cells increased anchorage-independent growth (16). RUNX2 is an oncogene that plays an important role in the progression and metastasis of several human cancers (27-29,69). Cancer

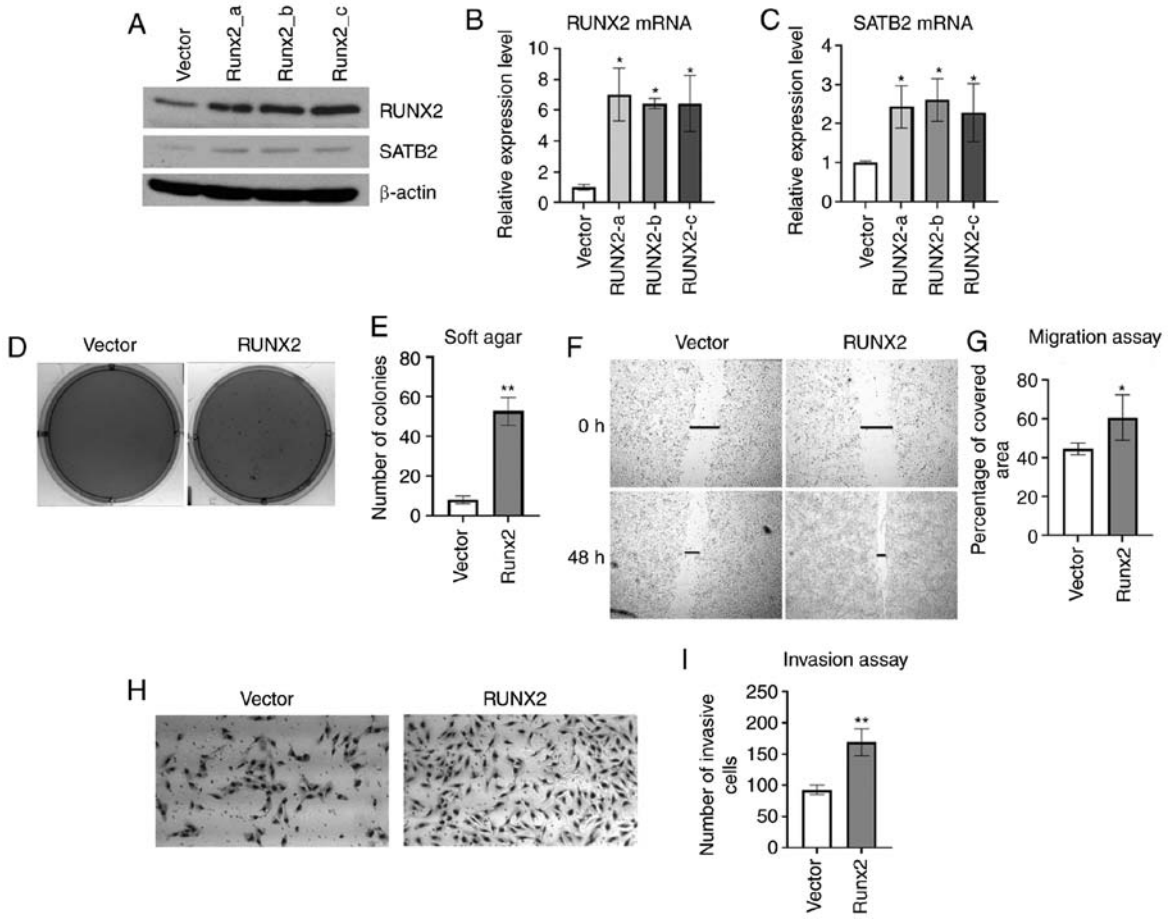

Figure 2. Overexpression of RUNX2 increases cancer hallmarks in BEAS-2B cells. (A-C) Expression levels of RUNX2 and SATB2 protein and mRNA in BEAS-2B cells stably transfected with RUNX2 vector compared with empty vector control were determined by western blotting and reverse transcription-quantitative PCR assays. (D and E) Soft agar assays of BEAS-2B cells ectopically expressing RUNX2 compared with vector control, and quantified number of colonies in agars of each group by ImageJ software. (F and G) Cell migration ability of BEAS-2B cells ectopically expressing RUNX2 was measured by scratch wound healing assays and the images were captured at a magnification of x20. Quantification of the wound healing rate was conducted by measuring the percentage of wound area covered for each group during 48 h using ImageJ software. (H and I) The invasion of BEAS-2B cells ectopically expressing RUNX2 was measured by Transwell assay and the images were captured at a magnification of x40. The number of invasive cells was counted using ImageJ and compared with the control. Statistical significance was calculated by the GraphPad Prism software using ANOVA for comparisons among groups. *P<0.05 and **P<0.01. RUNX2, runt-related transcription factor 2; SATB2, AT-rich sequence-binding protein 2.

hallmarks were examined in BEAS-2B cells stably expressing RUNX2. To assess whether this was sufficient to promote transformation, BEAS-2B cells overexpressing RUNX2 that were cultured in soft agar demonstrated increased colony growth compared with an empty vector control (Fig. 2D and E). Overexpression of RUNX2 in BEAS-2B cells also promoted acceleration of wound healing and cell invasion compared with an empty vector control (Fig. 2F-I). These findings indicated that RUNX2 induced cancer hallmarks in BEAS-2B cells by inducing SATB2.

Inhibition of RUNX2 activity in Ni-transformed BEAS-2B cells eliminates cancer hallmarks. Previous studies have reported the role of RUNX2 in lung cancer and inhibition of RUNX2 has been revealed to suppress tumorigenesis in lung cancer cells (70-72). A previous study using computer-assisted drug design (CADD) screening detected a novel inhibitor of RUNX2 transcriptional activity termed CADD522 (73-75). This inhibitor was used in Ni-T cells to investigate whether inhibition of RUNX2 activity can suppress cancer-related properties. Cell viability and cytotoxicity were assessed by treating BEAS-2B cells for 24 h at 0-150 μM of CADD522. There was no loss of cell viability or increased cytotoxicity at 50 μM of CADD522 for 24 h (Fig. 3A and B). Since BEAS-2B cells tolerated a dose of 50 μM, this dose was selected for further studies. To confirm that RUNX2 activity can be suppressed by CADD522, Ni-T cells were treated with 50 μM CADD522 for 24 h. RUNX2 mRNA and protein levels were not significantly reduced in treated BEAS-2B or Ni-T cells (Fig. 3C and D). However downstream target genes of RUNX2, VEGF and BSP were significantly inhibited by 50 μM CADD522 treatment for 24 h in Ni-T cells (Fig. 3E-F). In addition, SIRT6 (sirtuin 6), that was negatively regulated by RUNX2, was increased by CADD522 (Fig. 3G), indicating that CADD522 repressed RUNX2 trans-activity. SATB2 mRNA and protein were also found reduced in Ni-T cells treated with 50 μM CADD522 (Fig. 3H and I).

The anchorage independent growth of cells was analyzed by culturing Ni-T cells in soft agar containing 50 μM CADD522 for 4 weeks. The colony number and size were significantly reduced in CADD522-treated Ni-T cells compared with control (Fig. 3J and K). The metastatic potential of Ni-T treated with CADD522 was assessed in cell invasion and migration assays.

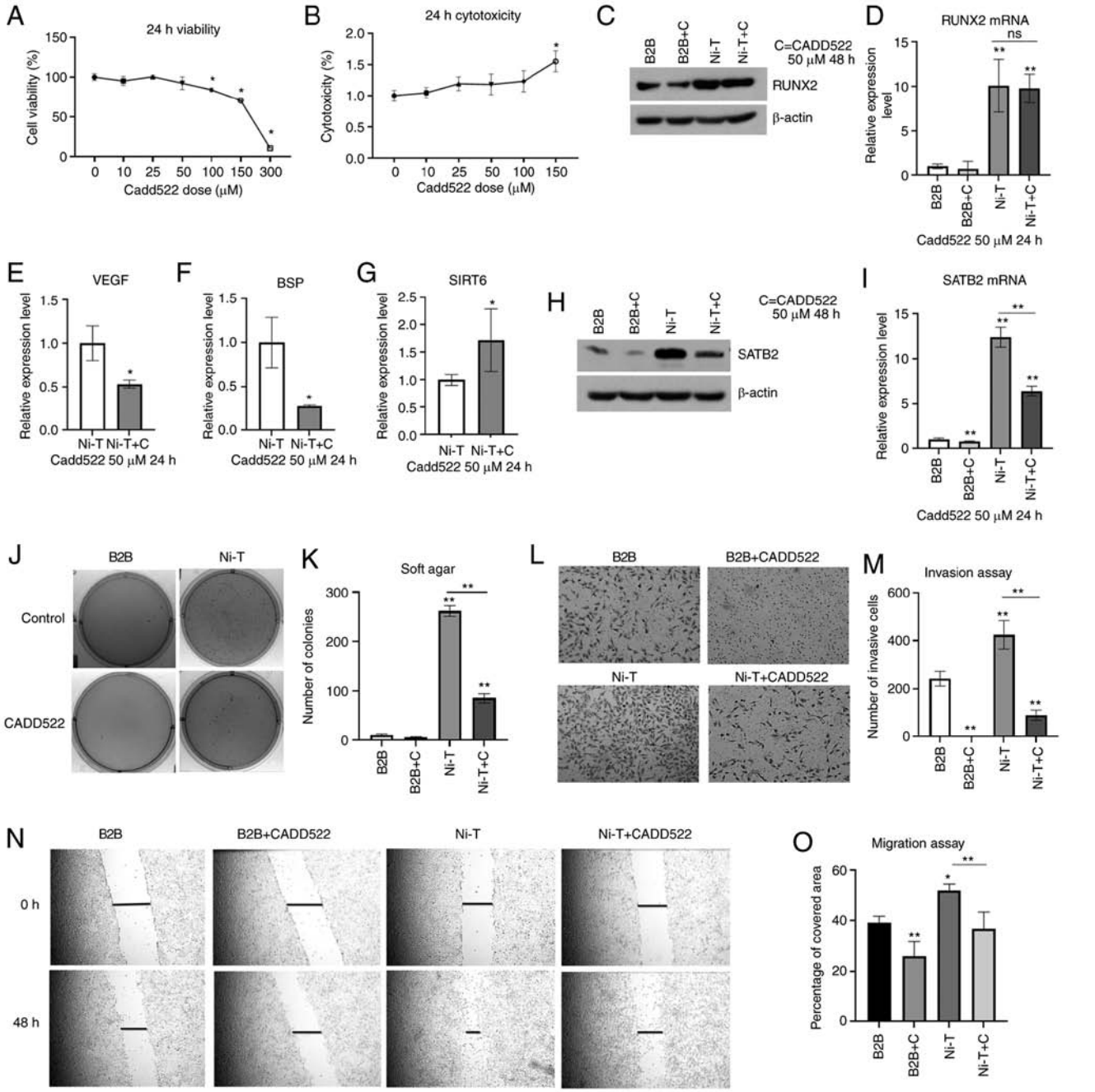

Figure 3. Inhibition of RUNX2 activity in Ni-T BEAS-2B cells reverses cancer hallmarks. (A and B) Cell viability and cytotoxicity assays in BEAS-2B cells treated with CADD522 for 24 h. (C and D) The expression levels of RUNX2 protein and mRNA in CADD522-treated BEAS-2B cells and Ni-T cells by western blotting and RT-qPCR assays. (E-G) The expression level of RUNX2 downstream genes, VEGF, BSP, and SIRT6 mRNA in Ni-T cells treated with 50 μM CADD522 by RT-qPCR. (H and I) The expression level of SATB2 protein and mRNA in BEAS-2B cells and Ni-T cells treated with 50 μM CADD522 by western blotting and RT-qPCR assays. (J and K) Soft agar assay of BEAS-2B cells and Ni-T cells treated with CADD522 at 50 μM and compared with that treated with control. (L and M) The invasion of BEAS-2B cells and Ni-T cells treated with CADD522 at 50 μM was measured by Transwell assay and images were captured at a magnification of x20. (N and O) Cell migration ability in BEAS-2B cells Ni-T cells with inhibited RUNX2 activity was measured by scratch wound healing assays, and images were captured at a magnification of x20. Statistical significance was calculated by the GraphPad Prism software using ANOVA for comparisons among groups. *P<0.05 and **P<0.01. RUNX2, runt-related transcription factor 2; Ni-T, Ni-transformed; RT-qPCR, reverse transcription-quantitative PCR; VEGF, vascular epithelial growth factor; BSP, bone sialoprotein; SIRT6, sirtuin 6; SATB2, AT-rich sequence-binding protein 2.

As revealed in Fig. 3L and M, CADD522-treated Ni-T cells demonstrated reduced wound healing rate and invasion as compared with the control.

Knockdown of RUNX2 prevents Ni-induced transformation in BEAS-2B cells. To further study the role of RUNX2 in Ni-induced BEAS-2B transformation, RUNX2 was knocked down in normal BEAS-2B cells by shRNA stable transfection prior to a chronic exposure to Ni (Fig. 4A and B). $NiCl_2$ and $NiSO_4$ are two common soluble forms of Ni compounds used in cell transformation studies (7,57-63). The RUNX2-knockdown cells experienced massive cell death after treatment of 0.25 mM $NiCl_2$ for 2 weeks. Thus, a lower dose and a longer treatment time were tried with this compound. Cells were treated with

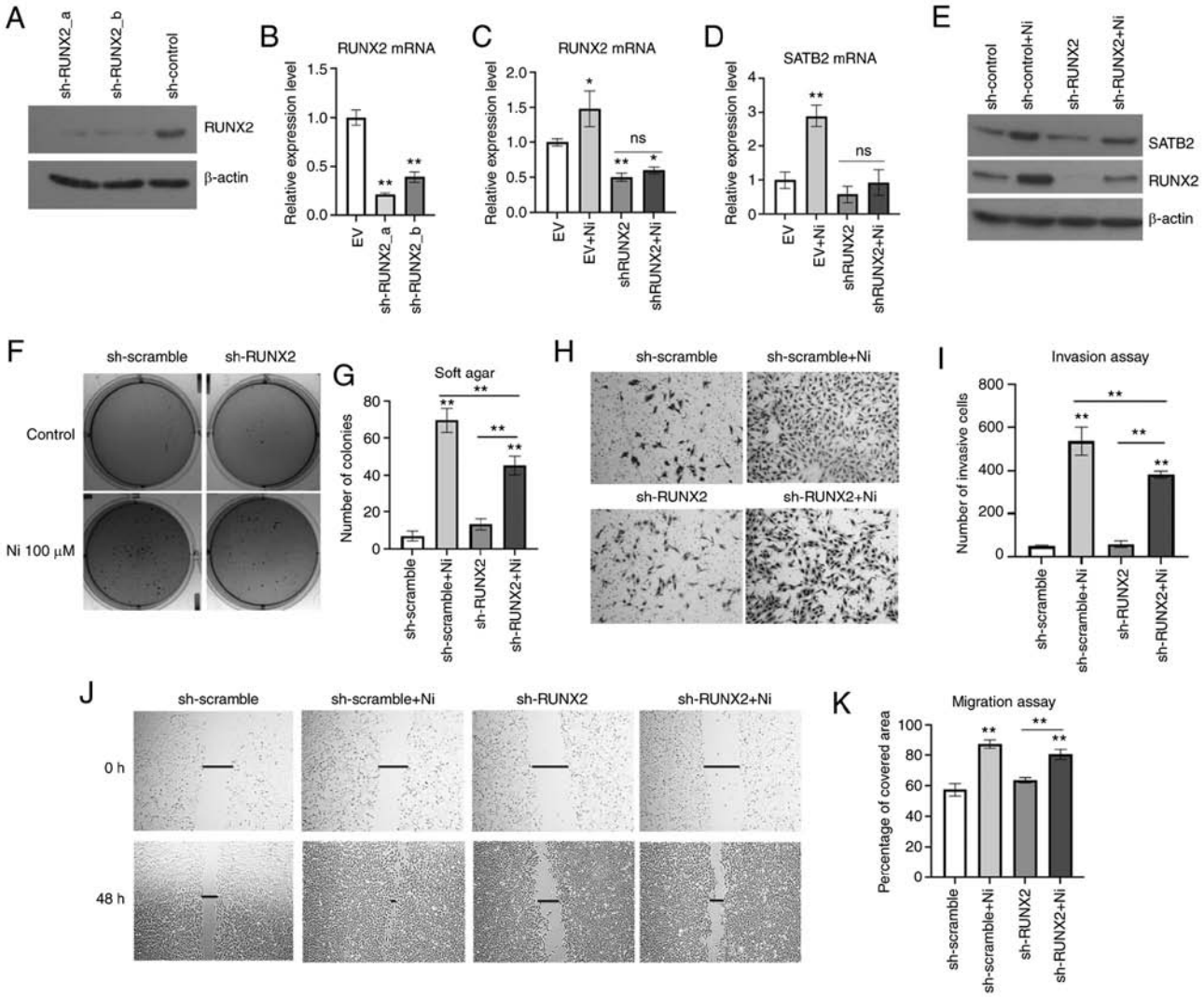

Figure 4. Knockdown of RUNX2 prevents SATB2 induction by Ni in BEAS-2B. (A and B) The protein and mRNA levels of RUNX2 were measured by western blotting and RT-qPCR assays after knockdown of RUNX2 by shRNA stable transfection in BEAS-2B cells. (C-E) The expression of RUNX2 and SATB2 protein and mRNA levels was measured by western blotting and RT-qPCR assays in BEAS-2B RUNX2-knockdown cells. (F and G) Soft agar assays of RUNX2-knockdown cells compared with scramble controls. (H and I) The invasion of RUNX2-knockdown cells was measured by Transwell assay and images were captured at a magnification of x20. The number of invading cells was counted using ImageJ software and compared with the control. (J and K) Cell migration ability in RUNX2-knockdown cells was measured by scratch wound healing assays and images were captured at a magnification of x20. The wound healing rate was analyzed by measuring the percentage of wound area covered for each group using ImageJ software. Statistical significance was calculated by the GraphPad Prism software using ANOVA for comparisons among groups. *P<0.05 and **P<0.01. RUNX2, runt-related transcription factor 2; SATB2, AT-rich sequence-binding protein 2; RT-qPCR, reverse transcription-quantitative PCR; sh-, short hairpin; ns, no significance.

100 μM $NiCl_2$ for 6 consecutive weeks to induce cell transformation. As demonstrated in Fig. 4C-E, the scramble control cells demonstrated significantly higher levels of RUNX2 compared with shRUNX2-transfected cells. Chronic exposure to Ni induced both RUNX2 and SATB2 level in control cells, while in RUNX2-knockdown cells, Ni failed to increase the levels of RUNX2 or SATB2 compared with controls. These results indicated that inhibition of RUNX2 decreased the induction of SATB2 by Ni chronic exposure.

Ni-induced cancer hallmarks were investigated in BEAS-2B cells harboring knockdown of RUNX2. As revealed in Fig. 4F and G, Ni-treated BEAS-2B cells with knockdown of RUNX2 demonstrated significantly reduced anchorage-independent growth compared with the control. Although knockdown of RUNX2 only slightly reduced cell migration of BEAS-2B cells chronically treated with Ni (Fig. 4H and I), Ni-treated cells with knockdown of RUNX2 demonstrated a reduced invasiveness (Fig. 4J and K). These findings indicated that RUNX2 was essential in maintaining the cancer hallmarks of Ni-T cells, which was likely dependent on SATB2.

miR-31 connects RUNX2 and SATB2 in Ni-induced cell transformation. SATB2 is maintained at low levels in most mature organisms, and it is regulated by post-transcriptional modifications and several miRNAs (48,76). miR-31 is a negative regulator for SATB2 (22,38,40,41). In a previous study, it was demonstrated that arsenic induced SATB2 level by inhibiting miR-31 in BEAS-2B cells (40). miR-31 could directly target SATB2 at the 3' UTR to diminish SATB2 mRNA stability and translation (22,41). miR-31 has also been revealed to be downstream of RUNX2 during osteogenic differentiation (22).

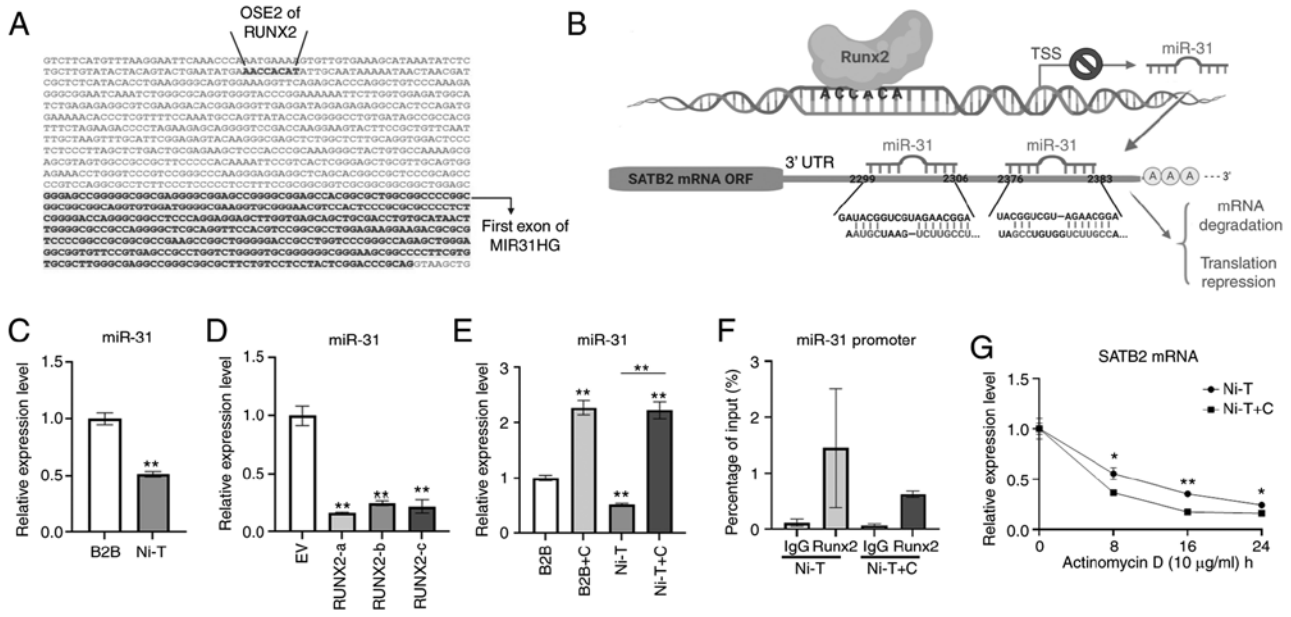

Figure 5. miR-31 connects RUNX2 and SATB2 signaling in Ni-T BEAS-2B cells. (A) Analysis of miR-31 promoter sequence and identification of RUNX2 core binding site by Ensembl. (B) An illustration of RUNX2 binding to the genomic miR-31 promoter region and an illustration of miR-31 targeting SATB2 mRNA 3' UTR at two target positions by TargetScan. (C) The level of miR-31 in Ni-T cells compared with normal BEAS-2B by RT-qPCR analysis. (D) The level of miR-31 in BEAS-2B cells ectopically expressing RUNX2 compared with vector control by RT-qPCR analysis. (E) The expression level of miR-31 in Ni-T cells treated by CADD522 at 50 μM for 24 h compared with that in BEAS-2B cells by RT-qPCR analysis. (F) Chromatin immunoprecipitation analysis for RUNX2 binding at miR-31 promoter affected by CADD522 using primer that amplified the core binding site of RUNX2 at miR-31 promoter region. (G) RNA stability assay using actinomycin D to inhibit DNA transcription to assess the SATB2 mRNA degradation in CADD522-treated Ni-T cells by RT-qPCR. Statistical significance was calculated by the GraphPad Prism software using ANOVA for comparisons among groups. *P<0.05 and **P<0.01. miR, microRNA; RUNX2, runt-related transcription factor 2; SATB2, AT-rich sequence-binding protein 2; Ni-T, Ni-transformed; UTR, untranslated region; RT-qPCR, reverse transcription-quantitative PCR.

It connects RUNX2 and SATB2 by acting as a direct target of RUNX2 and an upregulator of SATB2 in osteogenesis and carcinogenesis. A search of the promoter of miR-31 on Ensembl genome browser revealed a core binding sequence for RUNX2 upstream of TSS of miR-31 (Fig. 5A). An illustration of RUNX2 binding at the miR-31 promoter region and inhibiting its transcription is demonstrated in Fig. 5B. Furthermore, miR-31 complementary base pairing was revealed with the sequence on SATB2 mRNA 3' UTR region to mediate its mRNA degradation and translation repression and two target sites on 3' UTR of SATB2 mRNA were identified by TargetScan.

The expression level of miR-31 in Ni-T cells was reduced compared with normal BEAS-2B cells (Fig. 5C). To confirm whether miR-31 was regulated by RUNX2, BEAS-2B cells overexpressing RUNX2 and CADD522-treated Ni-T cells were subjected to miRNA extraction and qPCR analysis for the expression level of miR-31. Overexpression of RUNX2 in BEAS-2B cells reduced the expression level miR-31 compared with the vector control (Fig. 5D), while increased miR-31 expression levels were observed in Ni-T cells and BEAS-2B cells with inhibited RUNX2 activity (Fig. 5E). The physical binding of RUNX2 to the core binding site on miR-31 promoter was demonstrated by Deng *et al* (22). To further investigate the mechanism by which CADD522 induced the expression level of miR-31, the binding of RUNX2 at the core binding site of miR-31 promotor region was examined by ChIP in Ni-T cells. A primer that spans the binding site in the promoter of miR-31 was used for qPCR analysis and another primer spanning an unrelated promoter region was used as a negative control. The binding of RUNX2 to miR-31 promoter was confirmed. Upon treatment with CADD522, the binding of RUNX2 was slightly reduced as compared with control (Fig. 5F), indicating that CADD522 alleviated the inhibitory effect by RUNX2 on miR-31 promoter and thereby increased the expression level of miR-31.

It is known that miRNAs target downstream mRNAs by promoting mRNA degradation and reducing translation (77). Since CADD52 induced expression of miR-31, an inhibition of DNA transcription by actinomycin D in CADD522-treated Ni-T cells was conducted to assess the stability of SATB2 mRNA. CADD522-treated Ni-T cells had less SATB2 mRNA stability compared with the control (Fig. 5G), indicating that increased SATB2 mRNA degradation was the operative event. These findings indicated that RUNX2 increased SATB2 by suppressing the expression of miR-31, since RUNX2 directly targeted miR-31 promoter to negatively regulate its expression, and miR-31 was hypothesized to contribute to decreased stability of SATB2 mRNA in Ni-T cells.

Overexpression of miR-31 represses Ni-induced cancer hallmarks. miRNAs target downstream mRNAs by base-paring with a complementary sequence on their 3' UTR, while the levels of target mRNAs are not necessarily affected by miRNAs. Genes not affected by the binding of targeting miRNAs are termed tuning genes, and those that can be turned off by the binding of miRNAs are termed switch genes (44,78). To investigate whether miR-31 regulates the level of SATB2

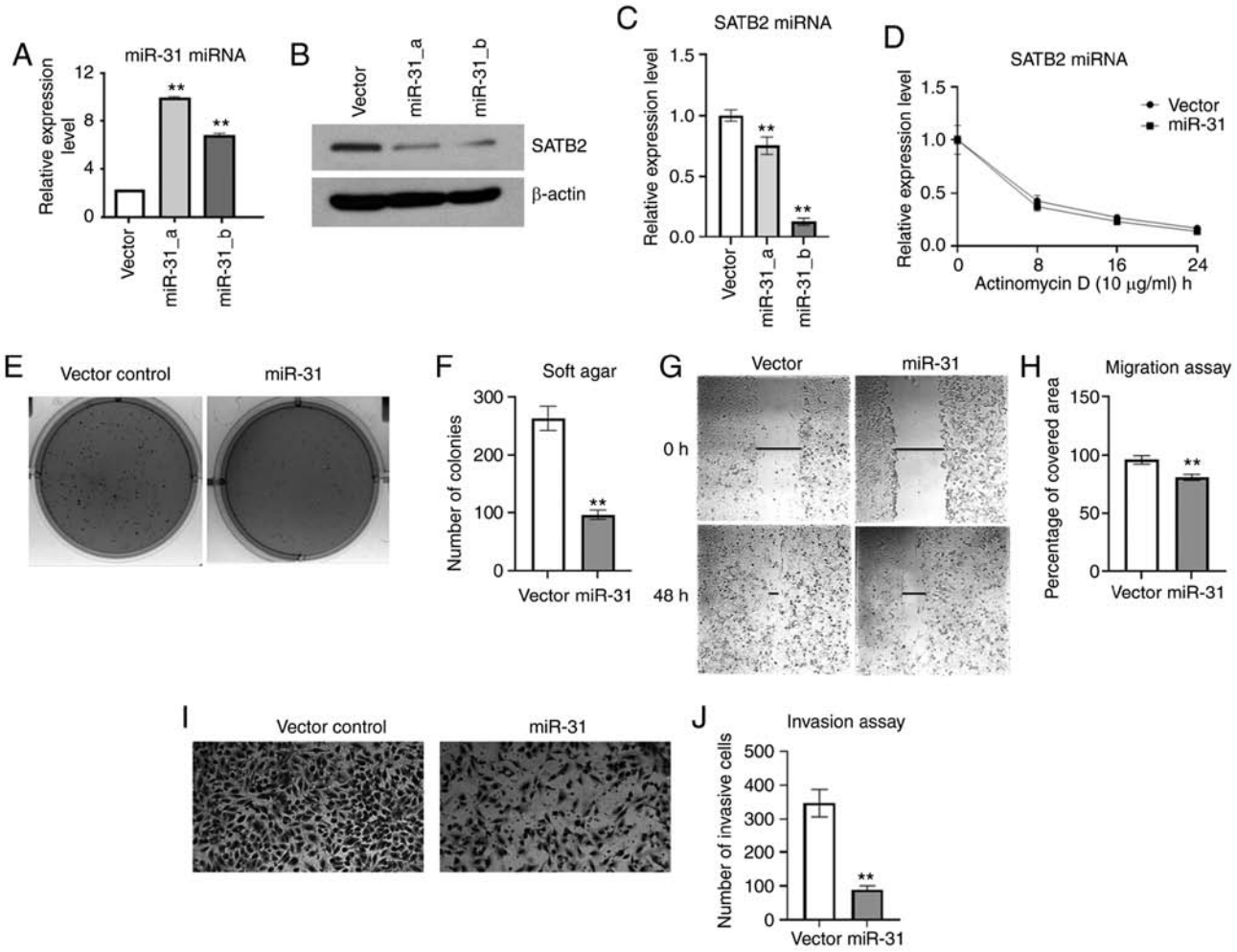

Figure 6. Overexpression of miR-31 in Ni-transformed BEAS-2B cells suppresses Ni-induced cancer hallmarks. (A) Ectopic expression of miR-31 in Ni-T cells by stable transfection and the expression level of miR-31 was measured by RT-qPCR analysis. (B and C) The level of SATB2 mRNA and protein in Ni-T cells ectopically expressing miR-31 by western blotting and RT-qPCR analysis. (D) RNA stability assay using actinomycin D to examine the SATB2 mRNA degradation in miR-31-knockdown BEAS-2B cells. (E and F) Soft agar assays of Ni-T cells ectopically expressing miR-31 compared with controls. (G and H) Cell migration ability in Ni-T cells ectopically expressing miR-31 was measured by scratch tests and images were taken at a magnification of x20. The wound healing rate was analyzed by measuring the percentage of wound area covered for each group using ImageJ software. (I and J) The invasion of Ni-T cells ectopically expressing miR-31 was measured by Transwell assay and the images were captured at a magnification of x40. The number of invading cells was counted using ImageJ software and compared with the control. Statistical significance was calculated by the GraphPad Prism software using ANOVA for comparisons among groups. **P<0.01. miR, microRNA; RT-qPCR, reverse transcription-quantitative PCR; SATB2, AT-rich sequence-binding protein 2; Ni-T, Ni-transformed.

in Ni-T cells, miR-31 was ectopically expressed (Fig. 6A). SATB2 protein and mRNA expression levels were measured by western blotting and qPCR. As revealed in Fig. 6B and C, ectopically expressed miR-31 in Ni-T cells suppressed the protein and mRNA levels of SATB2. However, unlike CADD522 which promoted SATB2 mRNA degradation, the stability of SATB2 mRNA was not significantly impaired in miR-31 overexpressed cells compared with vector control (Fig. 6D). This may be due to suppressed transcription of miR-31 under the treatment of actinomycin D, failing to show the direct link between miR-31 and SATB2.

Since exogenous expression of miR-31 in Ni-T cells reduced SATB2 levels, and knockdown of SATB2 was revealed to reduce cell transformation (16), it was hypothesized that cell transformation and metastasis would also be inhibited in Ni-T cells stably expressing exogenous miR-31. The colony number and size in soft agar were significantly decreased in miR-31-overexpressing cells compared with the vector control as demonstrated in Fig. 6E and F. To investigate whether the expression of miR-31 in Ni-T cells also suppressed cellular metastasis, both migration and invasion were analyzed using the scratch test and invasion assay, respectively. As demonstrated in Fig. 6G and H, the wound healing rate was reduced in Ni-T cells ectopically expressing miR-31 compared with the control, indicating a decreased cell migration ability. The number of invasive cells was also significantly reduced in miR-31-overexpressed cells (Fig. 6I and J). Collectively, overexpression of miR-31 reduced cell transformation and metastatic potential in Ni-T cells, indicating that miR-31 could be a critical regulator in Ni-induced cell transformation by its effects on SATB2 expression.

Inhibition of miR-31 increases cancer hallmarks in BEAS-2B cells. To further examine the role of miR-31 in cell transformation, miR-31 was knocked down in BEAS-2B cells by shRNA (Fig. 7A). The mRNA and protein levels of SATB2

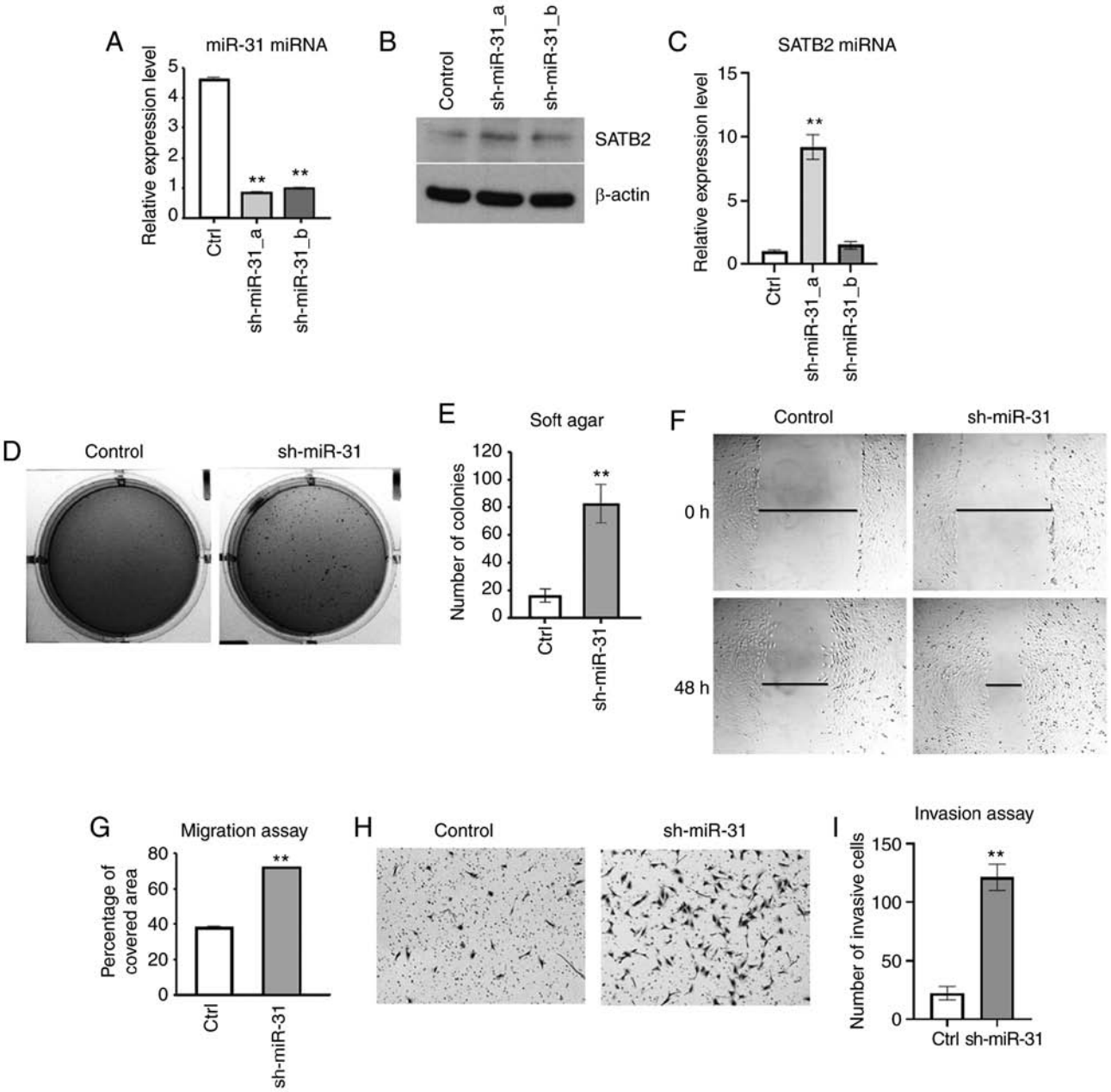

Figure 7. Knockdown of miR-31 promotes cancer hallmarks in BEAS-2B cells. (A) Knockdown of miR-31 in BEAS-2B cells by miR-31 inhibitor and the expression level of miR-31 was measured by RT-qPCR analysis. (B and C) The levels of SATB2 mRNA and protein in miR-31-knockdown BEAS-2B cells were determined by western blotting and RT-qPCR analysis. (D and E) Soft agar assays of miR-31-knockdown cells and the quantification of the number of colonies compared with that of the control. (F and G) Cell migration ability in miR-31-knockdown cells was measured by scratch tests and the images were captured at a magnification of x20. The wound healing rate was analyzed by measuring the percentage of wound area covered for each group using ImageJ software. (H and I) The invasion of miR-31-knockdown cells was measured by Transwell assay and images were captured at a magnification of x20. The number of invasive cells was counted using ImageJ and was compared with the control. GraphPad Prism software using ANOVA for comparisons among groups. **P<0.01. miR, microRNA; RT-qPCR, reverse transcription-quantitative PCR; SATB2, AT-rich sequence-binding protein 2; sh-, short hairpin.

were increased in one of the clones of miR-31-knockdown BEAS-2B cells (Fig. 7B and C). Inhibition of miR-31 level in BEAS-2B cells significantly promoted anchorage-independent growth as compared with the scramble shRNA-transfected controls (Fig. 7D and E). The cell metastasis was investigated in BEAS-2B cells with knockdown of miR-31. Cells with reduced expression of miR-31 exhibited increased migration compared with the scramble shRNA control (Fig. 7F and G). Furthermore, knockdown of miR-31 effectively increased the invasiveness as compared with the control (Fig. 7H and I). Collectively, these results indicated that miR-31 played an important role in inhibiting cell transformation and metastasis in BEAS-2B cells.

Discussion

The present study proposed a signaling pathway, RUNX2/miR-31/SATB2, that drives Ni-induced BEAS-2B cell transformation. Expression of SATB2 and RUNX2 were both increased in Ni-transformed BEAS-2B cells (Ni-T) and miR-31 levels were reduced. Ectopic expression of RUNX2 in BEAS-2B cells promoted cancer hallmarks, while an inhibition

of RUNX2 in Ni-T cells or knockdown of RUNX2 in BEAS-2B cells prior to Ni treatment significantly prevented the induction of SATB2 as well as carcinogenesis. These results indicated an important role of RUNX2 in Ni-induced cell transformation, which is likely mediated by inducing the expression of SATB2. miR-31 was demonstrated to be an upstream negative regulator of SATB2 in arsenic-transformed BEAS-2B cells (40). miR-31 is targeted by RUNX2 at the promoter and its expression level was revealed to be regulated by RUNX2 in BEAS-2B cells. Knockdown of miR-31 in normal BEAS-2B cells increased SATB2 level and cancer hallmarks, while overexpression of miR-31 in Ni-T cells reversed transformation by decreasing SATB2. Different doses and treatment times for soluble Ni-induced cell transformation have been reported in numerous studies (7,57-63), however a dose-response effect of soluble Ni on cell growth, migration and invasion has not been well explored in the same detail and could be studied in the future. Furthermore, a dose-response relationship between soluble Ni exposure and expression levels of these components will be explored in future studies. Collectively, these results indicated that long-term soluble $NiSO_4$ exposure induced SATB2 expression through the induction of RUNX2 and inhibition of miR-31 which is a mechanism for Ni-induced BEAS-2B cell transformation.

Ni-induced cell transformation occurs through several mechanisms, including the hypoxia-inducible signaling pathway, epigenetic changes including DNA methylation, histone acetylation and miRNA regulation, tumor suppressor gene loss and oncogene activation (79). Hypoxia-inducible factor (HIF) is a heterodimeric transcriptional factor that consists of 2 subunits, HIF-1α and HIF-1β, both of which are required for HIF-1 to function; HIF-1β is integral in HIF-1 heterodimer formation, while HIF-1α is the key regulatory subunit and is responsible for HIF-1 transcriptional activity (80). Previous studies demonstrated that Ni could replace iron in the HIF prolyl hydroxylases and thus inhibit the association of HIF-1α with Von-Hippel-Lindau (VHL) E3 ubiquitin ligase, which in turn stabilizes HIF protein (81-83). RUNX2 was also revealed to cause accumulation of HIF-1α protein in chondrocytes since it stabilizes HIF-1α by competition with pVHL at the oxygen-dependent degradation domain (ODDD) of HIF-1α and prevents HIF-1α ubiquitination (84). Another study confirmed the physical binding of the Runt domain of RUNX2 with HIF-1α and indicated that RUNX2 and HIF-1α interaction induced the expression of the downstream gene vascular epithelial growth factor (VAGF) (85). Recently SATB2 was also revealed to regulate HIF-1a expression under hypoxia signaling and mediate cell stemness, proliferation and cell survival in oral squamous cell carcinoma (86). These findings indicated that both RUNX2 and SATB2 may also be involved in the mechanism of the Ni-induced hypoxia signaling pathway.

Carcinogenic mechanisms induced by Ni can ultimately lead to the activation of proto-oncogenes or inactivation of tumor suppressor genes such as p53 (87-89). SATB2 was reported to be an oncogene in numerous cancers (48). SATB2 was indicated as a diagnostic marker for CRC since SATB2 stained positively in 71-97% of primary and metastatic CRC biopsies (90). A reduced expression level of SATB2 in colon cancer was associated with poor prognosis, while increased SATB2 expression enhanced therapeutic sensitivity (90-94). A previous study demonstrated that SATB2 induction and subsequent transformation of colon epithelial cells (CRL-1831) was mediated through Wnt/β-catenin/T-cell factor (TCF)/lymphoid enhancer factor (LEF) pathway (13). Numerous downstream genes of the pathway have been associated with carcinogenesis, including c-Myc and VEGF (95). In fact, these genes are also downstream of RUNX2 (96,97). RUNX2 has been linked with SATB2 by numerous osteo-specific markers and miRNAs during bone development and carcinogenesis (19,20,22-25,39).

RUNX2 was indicated to be a novel prognostic marker in non-small cell lung cancer (NSCLC) since its expression was revealed to be tightly related with tumor size, stage, and lymph node metastasis (72). The present study focused on the role of RUNX2 in Ni-T cells and confirmed that RUNX2 is an upstream regulator of SATB2, and it is important in mediating cell transformation induced by Ni. Inhibition of RUNX2 was achieved by two methods in the present study, a small molecule inhibitor and gene knockdown. The advantage of small molecule drugs is functioning rapidly, continuously, and often reversibly across cell types and species (98) From a clinical point of view, it has the potential for therapeutic development, and the results of the present study could possibly add meaning to it. A concern in the use of small molecule inhibitors of RUNX2 would be its off-target effects. A previous study has demonstrated that CADD522 is specific for the RUNX family and highly specific in targeting RUNX2 transcriptional activity (75). Stable knockdown of RUNX2 by shRNA in normal BEAS-2B cells was carried out to provide further evidence that RUNX2 is critical in maintaining cancer hallmarks during Ni-induced transformation. Although SATB2 is considered a tumor suppressor for NSCLC (99), SATB2 levels increased in Ni-T BEAS-2B cells. In addition, inhibition of the expression level of SATB2 in Ni-T cells reduced cell proliferation and anchorage-independent growth (100). SATB2 was also induced by arsenic in BEAS-2B transformed cells, and this induction was demonstrated to be achieved by down-regulated miR-31, which was required to induce malignant transformation of BEAS-2B cells (40).

RUNX2 acts as an upstream regulator of miR-31 by directly targeting its promoter region in bone marrow mesenchymal stem cells (22). The expression level of miR-31 was negatively regulated by RUNX2 following Ni-transformation, and the binding of RUNX2 at miR-31 promoter was demonstrated. miR-31 is a negative regulator of SATB2 since overexpression of miR-31 suppressed SATB2 level in Ni-T cells, while inhibition of miR-31 restored SATB2 to normal low levels. miRNAs function by binding to the 3' UTR of target mRNAs and subsequently mediate mRNA de-capping, triggering degradation, as well as reducing mRNA translation (101). SATB2 mRNA was directly targeted by miR-31 in CRC and breast cancer cells (38,53). In the present study, it was observed that miR-31 affected SATB2 levels, and further studies on the mechanism by which miR-31 regulates SATB2 in this pathway are required.

Two target sequences that miR-31 bind to the 3' UTR of SATB2 mRNA were identified. Inhibition of RUNX2 transcriptional activity by CADD522 increased miR-31 levels, reducing the half-life of SATB2 mRNA, indicating that miR-31 promoted SATB2 mRNA degradation. miR-31 is a

highly evolutionarily conserved miRNA and its expression was revealed to be disrupted in the progression of numerous cancers and diseases such as psoriasis and systemic lupus erythematosus (102). The transcriptional regulation of miR-31 is suppressed in breast, prostate, liver, leukemia, and melanoma cancers, and this is partly mediated by hypermethylation of a CpG island in miR-31 promoter (103-107). In fact, DNA methylation is the most prevalent epigenetic event in Ni-induced lung cancer (81,108-112). Ni elicited global hypermethylation and suppressed key tumor suppressor genes to induce senescence as part of its carcinogenic pathway (113). Ni was also revealed to alter the expression levels of numerous ncRNAs by regulating the activity of DNA methyltransferases (DMNTs) (47). The level of miR-31 was reduced in Ni-T cells, allowing SATB2 protein to be expressed. In addition, RUNX2/miR-31 may not be the only upstream signaling for SATB2-mediated carcinogenesis induced by Ni since RUNX2 and SATB2 are regulated by other miRNAs such as miR-23a/27a/24-2 in cancer cells (23).

The present study described a signaling pathway leading to increased SATB2 in Ni-induced BEAS-2B transformation. It demonstrated that induced expression of RUNX2 by Ni-suppressed miR-31 expression by silencing its promoter, thereby allowing SATB2 mRNA translation, and increasing the protein level of SATB2, leading to cell transformation. Since SATB2 is a common gene significantly induced by different heavy metals in BEAS-2B cells (7), it would be of interest to investigate whether this is a shared pathway for other metal-induced lung carcinogenesis in future studies.

Acknowledgements

Not applicable.

Funding

The present study was supported by the National Institutes of Health grants (grant nos. ES000260, ES023174, ES029359, ES030583 CA229234 and ES026138).

Availability of data and materials

All datasets generated or analyzed during this study are available from the corresponding author upon reasonable request.

Author's contributions

MC, YZ and AJ contributed to the conception and design of the study. AJ performed preliminary experiments to establish the methodology to assess RUNX2 and miR-31 expression in cells. QYC generated miR-31 overexpression and knockdown clones, confirmed that these clones had authentic overexpression and knockdown and conducted cell transformation assays for these clones. YZ performed all of the remaining experiments that are reported in the study. YZ, QYC and NR analyzed the data and produced the final images of the study using the software mentioned in the study. HS and NR provided technical support and data interpretation for the study. YZ prepared the first draft of the manuscript. YZ and MC revised the manuscript according to the comments from the reviewers and editors. HS also assisted in confirming and providing detailed methods of the study. MC supervised the preparation of the manuscript and was the PI on NIH grants that financially supported this publication. All authors have read and approved the submitted manuscript.

Ethics approval and consent to participate

Not applicable.

Patient consent for publication

Not applicable.

Competing interests

The authors declare that they have no competing interests.

References

1. Huvinen M and Pukkala E: Cancer incidence among Finnish ferrochromium and stainless steel production workers in 1967-2011: A cohort study. BMJ Open 3: e003819, 2013.
2. Grimsrud TK and Andersen A: Evidence of carcinogenicity in humans of water-soluble nickel salts. J Occup Med Toxicol 5: 7, 2010.
3. Andersen A, Berge SR, Engeland A and Norseth T: Exposure to nickel compounds and smoking in relation to incidence of lung and nasal cancer among nickel refinery workers. Occup Environ Med 53: 708-713, 1996.
4. Seilkop SK and Oller AR: Respiratory cancer risks associated with low-level nickel exposure: An integrated assessment based on animal, epidemiological, and mechanistic data. Regul Toxicol Pharmacol 37: 173-190, 2003.
5. Anttila A, Pukkala E, Aitio A, Rantanen T and Karjalainen S: Update of cancer incidence among workers at a copper/nickel smelter and nickel refinery. Int Arch Occup Environ Health 71: 245-250, 1998.
6. Moulin JJ, Clavel T, Roy D, Dananche B, Marquis N, Fevotte J and Fontana JM: Risk of lung cancer in workers producing stainless steel and metallic alloys. Int Arch Occup Environ Health 73: 171-180, 2000.
7. Clancy HA, Sun H, Passantino L, Kluz T, Munoz A, Zavadil J and Costa M: Gene expression changes in human lung cells exposed to arsenic, chromium, nickel or vanadium indicate the first steps in cancer. Metallomics 4: 784-793, 2012.
8. Savarese F, Davila A, Nechanitzky R, De La Rosa-Velazquez I, Pereira CF, Engelke R, Takahashi K, Jenuwein T, Kohwi-Shigematsu T, Fisher AG and Grosschedl R: Satb1 and Satb2 regulate embryonic stem cell differentiation and Nanog expression. Genes Dev 23: 2625-2638, 2009.
9. Magnusson K, de Wit M, Brennan DJ, Johnson LB, McGee SF, Lundberg E, Naicker K, Klinger R, Kampf C, Asplund A, *et al*: SATB2 in combination with cytokeratin 20 identifies over 95% of all colorectal carcinomas. Am J Surg Pathol 35: 937-948, 2011.
10. Jiang G, Cui Y, Yu X, Wu Z, Ding G and Cao L: miR-211 suppresses hepatocellular carcinoma by downregulating SATB2. Oncotarget 6: 9457-9466, 2015.
11. Cartularo L, Kluz T, Cohen L, Shen SS and Costa M: Molecular mechanisms of malignant transformation by low dose cadmium in normal human bronchial epithelial cells. PLoS One 11: e0155002, 2016.
12. Fukuhara M, Agnarsdottir M, Edqvist PH, Coter A and Ponten F: SATB2 is expressed in Merkel cell carcinoma. Arch Dermatol Res 308: 449-454, 2016.
13. Yu W, Ma Y, Shankar S and Srivastava RK: SATB2/β-catenin/TCF-LEF pathway induces cellular transformation by generating cancer stem cells in colorectal cancer. Sci Rep 7: 10939, 2017.
14. Bae T, Rho K, Choi JW, Horimoto K, Kim W and Kim S: Identification of upstream regulators for prognostic expression signature genes in colorectal cancer. BMC Syst Biol 7: 86, 2013.

15. Yu W, Ma Y, Shankar S and Srivastava RK: Role of SATB2 in human pancreatic cancer: Implications in transformation and a promising biomarker. Oncotarget 7: 57783-57797, 2016.
16. Wu F, Jordan A, Kluz T, Shen S, Sun H, Cartularo LA and Costa M: SATB2 expression increased anchorage-independent growth and cell migration in human bronchial epithelial cells. Toxicol Appl Pharmacol 293: 30-36, 2016.
17. Zhao X, Qu Z, Tickner J, Xu J, Dai K and Zhang X: The role of SATB2 in skeletogenesis and human disease. Cytokine Growth Factor Rev 25: 35-44, 2014.
18. Komori T: Regulation of skeletal development by the Runx family of transcription factors. J Cell Biochem 95: 445-453, 2005.
19. Nakashima K, Zhou X, Kunkel G, Zhang Z, Deng JM, Behringer RR and de Crombrugghe B: The novel zinc finger-containing transcription factor osterix is required for osteoblast differentiation and bone formation. Cell 108: 17-29, 2002.
20. Tang W, Li Y, Osimiri L and Zhang C: Osteoblast-specific transcription factor Osterix (Osx) is an upstream regulator of Satb2 during bone formation. J Biol Chem 286: 32995-33002, 2011.
21. Yu L, Xu Y, Qu H, Yu Y, Li W, Zhao Y and Qiu G: Decrease of miR-31 induced by TNF-α inhibitor activates SATB2/RUNX2 pathway and promotes osteogenic differentiation in ethanol-induced osteonecrosis. J Cell Physiol 234: 4314-4326, 2019.
22. Deng Y, Wu S, Zhou H, Bi X, Wang Y, Hu Y, Gu P and Fan X: Effects of a miR-31, Runx2, and Satb2 regulatory loop on the osteogenic differentiation of bone mesenchymal stem cells. Stem Cells Dev 22: 2278-2286, 2013.
23. Hassan MQ, Gordon JA, Beloti MM, Croce CM, van Wijnen AJ, Stein JL, Stein GS and Lian JB: A network connecting Runx2, SATB2, and the miR-23a~27a~24-2 cluster regulates the osteoblast differentiation program. Proc Natl Acad Sci USA 107: 19879-19884, 2010.
24. Dobreva G, Chahrour M, Dautzenberg M, Chirivella L, Kanzler B, Farinas I, Karsenty G and Grosschedl R: SATB2 is a multifunctional determinant of craniofacial patterning and osteoblast differentiation. Cell 125: 971-986, 2006.
25. Dowrey T, Schwager EE, Duong J, Merkuri F, Zarate YA and Fish JL: Satb2 regulates proliferation and nuclear integrity of pre-osteoblasts. Bone 127: 488-498, 2019.
26. Zhang J, Tu Q, Grosschedl R, Kim MS, Griffin T, Drissi H, Yang P and Chen J: Roles of SATB2 in osteogenic differentiation and bone regeneration. Tissue Eng Part A 17: 1767-1776, 2011.
27. Kayed H, Jiang X, Keleg S, Jesnowski R, Giese T, Berger MR, Esposito I, Lohr M, Friess H and Kleeff J: Regulation and functional role of the Runt-related transcription factor-2 in pancreatic cancer. Br J Cancer 97: 1106-1115, 2007.
28. Pratap J, Lian JB, Javed A, Barnes GL, van Wijnen AJ, Stein JL and Stein GS: Regulatory roles of Runx2 in metastatic tumor and cancer cell interactions with bone. Cancer Metastasis Rev 25: 589-600, 2006.
29. Niu DF, Kondo T, Nakazawa T, Oishi N, Kawasaki T, Mochizuki K, Yamane T and Katoh R: Transcription factor Runx2 is a regulator of epithelial-mesenchymal transition and invasion in thyroid carcinomas. Lab Invest 92: 1181-1190, 2012.
30. Thomas DM, Johnson SA, Sims NA, Trivett MK, Slavin JL, Rubin BP, Waring P, McArthur GA, Walkley CR, Holloway AJ, *et al*: Terminal osteoblast differentiation, mediated by runx2 and p27KIP1, is disrupted in osteosarcoma. J Cell Biol 167: 925-934, 2004.
31. Akech J, Wixted JJ, Bedard K, van der Deen M, Hussain S, Guise TA, van Wijnen AJ, Stein JL, Languino LR, Altieri DC, *et al*: Runx2 association with progression of prostate cancer in patients: Mechanisms mediating bone osteolysis and osteoblastic metastatic lesions. Oncogene 29: 811-821, 2010.
32. Sun X, Wei L, Chen Q and Terek RM: HDAC4 represses vascular endothelial growth factor expression in chondrosarcoma by modulating RUNX2 activity. J Biol Chem 284: 21881-21890, 2009.
33. Papachristou DJ, Papachristou GI, Papaefthimiou OA, Agnantis NJ, Basdra EK and Papavassiliou AG: The MAPK-AP-1/-Runx2 signalling axes are implicated in chondrosarcoma pathobiology either independently or via up-regulation of VEGF. Histopathology 47: 565-574, 2005.
34. Inman CK and Shore P: The osteoblast transcription factor Runx2 is expressed in mammary epithelial cells and mediates osteopontin expression. J Biol Chem 278: 48684-48689, 2003.
35. Baniwal SK, Khalid O, Gabet Y, Shah RR, Purcell DJ, Mav D, Kohn-Gabet AE, Shi Y, Coetzee GA and Frenkel B: Runx2 transcriptome of prostate cancer cells: Insights into invasiveness and bone metastasis. Mol Cancer 9: 258, 2010.
36. Yuen HF, Kwok WK, Chan KK, Chua CW, Chan YP, Chu YY, Wong YC, Wang X and Chan KW: TWIST modulates prostate cancer cell-mediated bone cell activity and is upregulated by osteogenic induction. Carcinogenesis 29: 1509-1518, 2008.
37. Aprelikova O, Yu X, Palla J, Wei BR, John S, Yi M, Stephens R, Simpson RM, Risinger JI, Jazaeri A and Niederhuber J: The role of miR-31 and its target gene SATB2 in cancer-associated fibroblasts. Cell Cycle 9: 4387-4398, 2010.
38. Yang MH, Yu J, Chen N, Wang XY, Liu XY, Wang S and Ding YQ: Elevated microRNA-31 expression regulates colorectal cancer progression by repressing its target gene SATB2. PLoS One 8: e85353, 2013.
39. Zhang Y, Xie RL, Croce CM, Stein JL, Lian JB, van Wijnen AJ and Stein GS: A program of microRNAs controls osteogenic lineage progression by targeting transcription factor Runx2. Proc Natl Acad Sci USA 108: 9863-9868, 2011.
40. Chen QY, Li J, Sun H, Wu F, Zhu Y, Kluz T, Jordan A, DesMarais T, Zhang X, Murphy A and Costa M: Role of miR-31 and SATB2 in arsenic-induced malignant BEAS-2B cell transformation. Mol Carcinog 57: 968-977, 2018.
41. Ge J, Guo S, Fu Y, Zhou P, Zhang P, Du Y, Li M, Cheng J and Jiang H: Dental follicle cells participate in tooth eruption via the RUNX2-miR-31-SATB2 Loop. J Dent Res 94: 936-944, 2015.
42. Li Z, Hassan MQ, Volinia S, van Wijnen AJ, Stein JL, Croce CM, Lian JB and Stein GS: A microRNA signature for a BMP2-induced osteoblast lineage commitment program. Proc Natl Acad Sci USA 105: 13906-13911, 2008.
43. Li Z, Hassan MQ, Jafferji M, Aqeilan RI, Garzon R, Croce CM, van Wijnen AJ, Stein JL, Stein GS and Lian JB: Biological functions of miR-29b contribute to positive regulation of osteoblast differentiation. J Biol Chem 284: 15676-15684, 2009.
44. Bartel DP: MicroRNAs: Genomics, biogenesis, mechanism, and function. Cell 116: 281-297, 2004.
45. Pawlicki JM and Steitz JA: Nuclear networking fashions pre-messenger RNA and primary microRNA transcripts for function. Trends Cell Biol 20: 52-61, 2010.
46. Lu J, Getz G, Miska EA, Alvarez-Saavedra E, Lamb J, Peck D, Sweet-Cordero A, Ebert BL, Mak RH, Ferrando AA, *et al*: MicroRNA expression profiles classify human cancers. Nature 435: 834-838, 2005.
47. Zhu Y, Chen QY, Li AH and Costa M: The role of non-coding RNAs involved in nickel-induced lung carcinogenic mechanisms. Inorganics 7: 81, 2019.
48. Chen QY, Des Marais T and Costa M: Deregulation of SATB2 in carcinogenesis with emphasis on miRNA-mediated control. Carcinogenesis 40: 393-402, 2019.
49. Tian W, Wang G, Liu Y, Huang Z, Zhang C, Ning K, Yu C, Shen Y, Wang M, Li Y, *et al*: The miR-599 promotes non-small cell lung cancer cell invasion via SATB2. Biochem Biophys Res Commun 485: 35-40, 2017.
50. El Bezawy R, Cominetti D, Fenderico N, Zuco V, Beretta GL, Dugo M, Arrighetti N, Stucchi C, Rancati T, Valdagni R, *et al*: miR-875-5p counteracts epithelial-to-mesenchymal transition and enhances radiation response in prostate cancer through repression of the EGFR-ZEB1 axis. Cancer Lett 395: 53-62, 2017.
51. Gu J, Wang G, Liu H and Xiong C: SATB2 targeted by methylated miR-34c-5p suppresses proliferation and metastasis attenuating the epithelial-mesenchymal transition in colorectal cancer. Cell Prolif 51: e12455, 2018.
52. Sun X, Liu S, Chen P, Fu D, Hou Y, Hu J, Liu Z, Jiang Y, Cao X, Cheng C, *et al*: miR-449a inhibits colorectal cancer progression by targeting SATB2. Oncotarget 8: 100975-100988, 2016.
53. Luo LJ, Yang F, Ding JJ, Yan DL, Wang DD, Yang SJ, Ding L, Li J, Chen D, Ma R, *et al*: miR-31 inhibits migration and invasion by targeting SATB2 in triple negative breast cancer. Gene 594: 47-58, 2016.
54. Gong Y, Xu F, Zhang L, Qian Y, Chen J, Huang H and Yu Y: MicroRNA expression signature for Satb2-induced osteogenic differentiation in bone marrow stromal cells. Mol Cell Biochem 387: 227-239, 2014.
55. Livak KJ and Schmittgen TD: Analysis of relative gene expression data using real-time quantitative PCR and the 2(-Delta Delta C(T)) method. Methods 25: 402-408, 2001.
56. Ratnadiwakara M and Änkö ML: mRNA stability assay using transcription inhibition by actinomycin D in mouse pluripotent stem cells. Bio-Protocol 8: e3072, 2018.
57. Costa M: Molecular mechanisms of nickel carcinogenesis. Annu Rev Pharmacol Toxicol 31: 321-337, 1991.

58. Chen QY and Costa M: A comprehensive review of metal-induced cellular transformation studies. Toxicol Appl Pharmacol 331: 33-40, 2017.
59. Huang H, Zhu J, Li Y, Zhang L, Gu J, Xie Q, Jin H, Che X, Li J, Huang C, *et al*: Upregulation of SQSTM1/p62 contributes to nickel-induced malignant transformation of human bronchial epithelial cells. Autophagy 12: 1687-1703, 2016.
60. Pang Y, Li W, Ma R, Ji W, Wang Q, Li D, Xiao Y, Wei Q, Lai Y, Yang P, *et al*: Development of human cell models for assessing the carcinogenic potential of chemicals. Toxicol Appl Pharmacol 232: 478-486, 2008.
61. Rani AS, Qu DQ, Sidhu MK, Panagakos F, Shah V, Klein KM, Brown N, Pathak S and Kumar S: Transformation of immortal, non-tumorigenic osteoblast-like human osteosarcoma cells to the tumorigenic phenotype by nickel sulfate. Carcinogenesis 14: 947-953, 1993.
62. Wang L, Fan J, Hitron JA, Son YO, Wise JT, Roy RV, Kim D, Dai J, Pratheeshkumar P, Zhang Z and Shi X: Cancer stem-like cells accumulated in nickel-induced malignant transformation. Toxicol Sci 151: 376-387, 2016.
63. Zhang Q, Salnikow K, Kluz T, Chen LC, Su WC and Costa M: Inhibition and reversal of nickel-induced transformation by the histone deacetylase inhibitor trichostatin A. Toxicol Appl Pharmacol 192: 201-211, 2003.
64. Borowicz S, Van Scoyk M, Avasarala S, Karuppusamy Rathinam MK, Tauler J, Bikkavilli RK and Winn RA: The soft agar colony formation assay. J Vis Exp e51998, 2014.
65. Jiang WG, Sanders AJ, Katoh M, Ungefroren H, Gieseler F, Prince M, Thompson SK, Zollo M, Spano D, Dhawan P, *et al*: Tissue invasion and metastasis: Molecular, biological and clinical perspectives. Semin Cancer Biol 35 Suppl: S244-S275, 2015.
66. Sahai E: Mechanisms of cancer cell invasion. Curr Opin Genet Dev 15: 87-96, 2005.
67. Komori T, Yagi H, Nomura S, Yamaguchi A, Sasaki K, Deguchi K, Shimizu Y, Bronson RT, Gao YH, Inada M, *et al*: Targeted disruption of Cbfa1 results in a complete lack of bone formation owing to maturational arrest of osteoblasts. Cell 89: 755-764, 1997.
68. Valenti MT, Serafini P, Innamorati G, Gili A, Cheri S, Bassi C and Dalle Carbonare L: Runx2 expression: A mesenchymal stem marker for cancer. Oncol Lett 12: 4167-4172, 2016.
69. Thomas DM, Carty SA, Piscopo DM, Lee JS, Wang WF, Forrester WC and Hinds PW: The retinoblastoma protein acts as a transcriptional coactivator required for osteogenic differentiation. Mol Cell 8: 303-316, 2001.
70. Bai X, Meng L, Sun H, Li Z, Zhang X and Hua S: MicroRNA-196b Inhibits cell growth and metastasis of lung cancer cells by targeting Runx2. Cell Physiol Biochem 43: 757-767, 2017.
71. Herreno AM, Ramirez AC, Chaparro VP, Fernandez MJ, Canas A, Morantes CF, Moreno OM, Bruges RE, Mejia JA, Bustos FJ, *et al*: Role of RUNX2 transcription factor in epithelial mesenchymal transition in non-small cell lung cancer lung cancer: Epigenetic control of the RUNX2 P1 promoter. Tumour Biol 41: 1010428319851014, 2019.
72. Li H, Zhou RJ, Zhang GQ and Xu JP: Clinical significance of RUNX2 expression in patients with nonsmall cell lung cancer: A 5-year follow-up study. Tumour Biol 34: 1807-1812, 2013.
73. Underwood KF, D'Souza DR, Mochin-Peters M, Pierce AD, Kommineni S, Choe M, Bennett J, Gnatt A, Habtemariam B, MacKerell AD Jr and Passaniti A: Regulation of RUNX2 transcription factor-DNA interactions and cell proliferation by vitamin D3 (cholecalciferol) prohormone activity. J Bone Miner Res 27: 913-925, 2012.
74. Underwood KF, Mochin MT, Brusgard JL, Choe M, Gnatt A and Passaniti A: A quantitative assay to study protein: DNA interactions, discover transcriptional regulators of gene expression, and identify novel anti-tumor agents. J Vis Exp 78: e50512, 2013.
75. Kim MS, Gernapudi R, Choi EY, Lapidus RG and Passaniti A: Characterization of CADD522, a small molecule that inhibits RUNX2-DNA binding and exhibits antitumor activity. Oncotarget 8: 70916-70940, 2017.
76. Dobreva G, Dambacher J and Grosschedl R: SUMO modification of a novel MAR-binding protein, SATB2, modulates immunoglobulin mu gene expression. Genes Dev 17: 3048-3061, 2003.
77. O'Brien J, Hayder H, Zayed Y and Peng C: Overview of MicroRNA biogenesis, mechanisms of actions, and circulation. Front Endocrinol (Lausanne) 9: 402, 2018.
78. Flynt AS and Lai EC: Biological principles of microRNA-mediated regulation: Shared themes amid diversity. Nat Rev Genet 9: 831-842, 2008.
79. Cameron KS, Buchner V and Tchounwou PB: Exploring the molecular mechanisms of nickel-induced genotoxicity and carcinogenicity: A literature review. Rev Environ Health 26: 81-92, 2011.
80. Lee JW, Bae SH, Jeong JW, Kim SH and Kim KW: Hypoxia-inducible factor (HIF-1)alpha: Its protein stability and biological functions. Exp Mol Med 36: 1-12, 2004.
81. Ke Q and Costa M: Hypoxia-inducible factor-1 (HIF-1). Mol Pharmacol 70: 1469-1480, 2006.
82. Li Q, Chen H, Huang X and Costa M: Effects of 12 metal ions on iron regulatory protein 1 (IRP-1) and hypoxia-inducible factor-1 alpha (HIF-1alpha) and HIF-regulated genes. Toxicol Appl Pharmacol 213: 245-255, 2006.
83. Davidson TL, Chen H, Di Toro DM, D'Angelo G and Costa M: Soluble nickel inhibits HIF-prolyl-hydroxylases creating persistent hypoxic signaling in A549 cells. Mol Carcinog 45: 479-489, 2006.
84. Lee SH, Che X, Jeong JH, Choi JY, Lee YJ, Lee YH, Bae SC and Lee YM: Runx2 protein stabilizes hypoxia-inducible factor-1α through competition with von Hippel-Lindau protein (pVHL) and stimulates angiogenesis in growth plate hypertrophic chondrocytes. J Biol Chem 287: 14760-14771, 2012.
85. Kwon TG, Zhao X, Yang Q, Li Y, Ge C, Zhao G and Franceschi RT: Physical and functional interactions between Runx2 and HIF-1α induce vascular endothelial growth factor gene expression. J Cell Biochem 112: 3582-3593, 2011.
86. Dong W, Chen Y, Qian N, Sima G, Zhang J, Guo Z and Wang C: SATB2 knockdown decreases hypoxia-induced autophagy and stemness in oral squamous cell carcinoma. Oncol Lett 20: 794-802, 2020.
87. Ali T, Mushtaq I, Maryam S, Farhan A, Saba K, Jan MI, Sultan A, Anees M, Duygu B, Hamera S, *et al*: Interplay of N acetyl cysteine and melatonin in regulating oxidative stress-induced cardiac hypertrophic factors and microRNAs. Arch Biochem Biophys 661: 56-65, 2019.
88. Clemens F, Verma R, Ramnath J and Landolph JR: Amplification of the Ect2 proto-oncogene and over-expression of Ect2 mRNA and protein in nickel compound and methylcholanthrene-transformed 10T1/2 mouse fibroblast cell lines. Toxicol Appl Pharmacol 206: 138-149, 2005.
89. Chiocca SM, Sterner DA, Biggart NW and Murphy EC Jr: Nickel mutagenesis: Alteration of the MuSVts110 thermosensitive splicing phenotype by a nickel-induced duplication of the 3' splice site. Mol Carcinog 4: 61-71, 1991.
90. Zhang YJ, Chen JW, He XS, Zhang HZ, Ling YH, Wen JH, Deng WH, Li P, Yun JP, Xie D and Cai MY: SATB2 is a promising biomarker for identifying a colorectal origin for liver metastatic adenocarcinomas. EBioMedicine 28: 62-69, 2018.
91. Dragomir A, de Wit M, Johansson C, Uhlen M and Ponten F: The role of SATB2 as a diagnostic marker for tumors of colorectal origin: Results of a pathology-based clinical prospective study. Am J Clin Pathol 141: 630-638, 2014.
92. Eberhard J, Gaber A, Wangefjord S, Nodin B, Uhlen M, Ericson Lindquist K and Jirstrom K: A cohort study of the prognostic and treatment predictive value of SATB2 expression in colorectal cancer. Br J Cancer 106: 931-938, 2012.
93. Lin F, Shi J, Zhu S, Chen Z, Li A, Chen T, Wang HL and Liu H: Cadherin-17 and SATB2 are sensitive and specific immunomarkers for medullary carcinoma of the large intestine. Arch Pathol Lab Med 138: 1015-1026, 2014.
94. Moh M, Krings G, Ates D, Aysal A, Kim GE and Rabban JT: SATB2 Expression distinguishes ovarian metastases of colorectal and appendiceal origin from primary ovarian tumors of mucinous or endometrioid type. Am J Surg Pathol 40: 419-432, 2016.
95. Yu W, Ma Y, Ochoa AC, Shankar S and Srivastava RK: Cellular transformation of human mammary epithelial cells by SATB2. Stem Cell Res 19: 139-147, 2017.
96. Shin MH, He Y, Marrogi E, Piperdi S, Ren L, Khanna C, Gorlick R, Liu C and Huang J: A RUNX2-Mediated epigenetic regulation of the survival of p53 defective cancer cells. PLoS Genet 12: e1005884, 2016.
97. Tang W, Yang F, Li Y, de Crombrugghe B, Jiao H, Xiao G and Zhang C: Transcriptional regulation of Vascular Endothelial Growth Factor (VEGF) by osteoblast-specific transcription factor Osterix (Osx) in osteoblasts. J Biol Chem 287: 1671-1678, 2012.
98. Efe JA and Ding S: The evolving biology of small molecules: Controlling cell fate and identity. Philos Trans R Soc Lond B Biol Sci 366: 2208-2221, 2011.

99. Ma YN, Zhang HY, Fei LR, Zhang MY, Wang CC, Luo Y and Han YC: SATB2 suppresses non-small cell lung cancer invasiveness by G9a. Clin Exp Med 18: 37-44, 2018.
100. Wei MM and Zhou GB: Long non-coding RNAs and their roles in non-small-cell lung cancer. Genomics Proteomics Bioinformatics 14: 280-288, 2016.
101. Valencia-Sanchez MA, Liu J, Hannon GJ and Parker R: Control of translation and mRNA degradation by miRNAs and siRNAs. Genes Dev 20: 515-524, 2006.
102. Stepicheva NA and Song JL: Function and regulation of microRNA-31 in development and disease. Mol Reprod Dev 83: 654-674, 2016.
103. Asangani IA, Harms PW, Dodson L, Pandhi M, Kunju LP, Maher CA, Fullen DR, Johnson TM, Giordano TJ, Palanisamy N and Chinnaiyan AM: Genetic and epigenetic loss of microRNA-31 leads to feed-forward expression of EZH2 in melanoma. Oncotarget 3: 1011-1025, 2012.
104. Augoff K, Das M, Bialkowska K, McCue B, Plow EF and Sossey-Alaoui K: miR-31 is a broad regulator of β1-integrin expression and function in cancer cells. Mol Cancer Res 9: 1500-1508, 2011.
105. Yamagishi M, Nakano K, Miyake A, Yamochi T, Kagami Y, Tsutsumi A, Matsuda Y, Sato-Otsubo A, Muto S, Utsunomiya A, *et al*: Polycomb-mediated loss of miR-31 activates NIK-dependent NF-κB pathway in adult T cell leukemia and other cancers. Cancer Cell 21: 121-135, 2012.
106. Ling H, Fabbri M and Calin GA: MicroRNAs and other non-coding RNAs as targets for anticancer drug development. Nat Rev Drug Discov 12: 847-865, 2013.
107. Kim HS, Lee KS, Bae HJ, Eun JW, Shen Q, Park SJ, Shin WC, Yang HD, Park M, Park WS, *et al*: MicroRNA-31 functions as a tumor suppressor by regulating cell cycle and epithelial-mesenchymal transition regulatory proteins in liver cancer. Oncotarget 6: 8089-8102, 2015.
108. Sakai T, Toguchida J, Ohtani N, Yandell DW, Rapaport JM and Dryja TP: Allele-specific hypermethylation of the retinoblastoma tumor-suppressor gene. Am J Hum Genet 48: 880-888, 1991.
109. Lee YW, Klein CB, Kargacin B, Salnikow K, Kitahara J, Dowjat K, Zhitkovich A, Christie NT and Costa M: Carcinogenic nickel silences gene expression by chromatin condensation and DNA methylation: A new model for epigenetic carcinogens. Mol Cell Biol 15: 2547-2557, 1995.
110. Ohtani-Fujita N, Fujita T, Aoike A, Osifchin NE, Robbins PD and Sakai T: CpG methylation inactivates the promoter activity of the human retinoblastoma tumor-suppressor gene. Oncogene 8: 1063-1067, 1993.
111. Sutcliffe JS, Nelson DL, Zhang F, Pieretti M, Caskey CT, Saxe D and Warren ST: DNA methylation represses FMR-1 transcription in fragile X syndrome. Hum Mol Genet 1: 397-400, 1992.
112. Greger V, Debus N, Lohmann D, Hopping W, Passarge E and Horsthemke B: Frequency and parental origin of hypermethylated RB1 alleles in retinoblastoma. Hum Genet 94: 491-496, 1994.
113. Hansen RS, Gartler SM, Scott CR, Chen SH and Laird CD: Methylation analysis of CGG sites in the CpG island of the human FMR1 gene. Hum Mol Genet 1: 571-578, 1992.